52. Organic Materials for Chemical Sensing

Asim K. Ray

Organic materials for chemical sensing are broadly classified into three categories: (i) macrocyclic compounds, (ii) conducting polymers, and (iii) cavitand molecules. A short review of current progress in inorganic sensing materials including graphene is given, pointing out their strengths and limitations. Principal wet techniques for depositing organic thin films are described and electrical, optical, and structural properties of all three types of organic materials are analyzed in relation to their importance in chemical sensing. Examples of recent advances in chemical sensing of different analytes and pollutants are presented.

The development of a new generation of sensors involves the study of fine-tuned sensor-active materials and transducers [52.1, 2]. Metal oxides, polymer/polymer composites, and dyes are regarded as key sensing materials. This chapter is organized into eight sections. The next section presents a summary of the needs for chemical sensing of different pollutants. The second section provides a brief description of different semiconducting oxide materials and their applications in sensor technology. Organized ultrathin organic films of molecular and polymeric semiconductors are currently the focus of considerable research with an emphasis on a molecular understanding of the sensing mechanisms. The low cost of fabrication, large-area processability, and widely diverse and tailorable physical, electronic, and optical properties have stimulated interest in their practical exploitation. Phthalocyanine and related macrocylic compounds have been extensively investigated for chemical sensing primarily because the desired functionality of phthalocyanine (Pc) molecules can be achieved by changing the central metal atom or by introducing substituents in their π-electron aromatic ring [52.3]. The third section is devoted to thin-film formulation of these interesting compounds and their structural, electrical, and optical properties relevant to sensing different types of pollutants. Important transduction methods and their applications in the development of practical sensors are presented in the fourth section, with an emphasis on the interaction at the analyte/film interface of macrocylic compounds. The ability of conducting polymers to change their physical properties during reaction with various redox agents makes them very useful for the development of gas sensors. The most common are polyaniline (PAni) and polypyrrole (PPY). It has been shown that the resistivity of polypyrrole increases in the presence of a reducing gas such as ammonia, but decreases in the presence of an oxidizing gas such as nitrogen dioxide. The

S. Kasap, P. Capper (Eds.), *Springer Handbook of Electronic and Photonic Materials*, DOI 10.1007/978-3-319-48933-9_52

gases cause a change in the near-surface charge-carrier density by reacting with surface-adsorbed oxygen ions [52.4]. Sensing properties of polymers and their importance in the development of intelligent sensors are described in Sect. 52.5. A class of supramolecules, called cavitands, that exhibit discotic phases depending on the structure, are shown to have potential for sensing applications [52.5]. Section 52.6 deals with the applications of thin films of these molecules such as calixresorcinarene for recognition of organic vapors. The chapter concludes by highlighting future development trends for sensor materials and technology in Sect. 52.7.

52.1 Analyte Requirements

The detection of pollutant gases and volatile organic compounds (VOC) whether in gaseous phase or dissolved in water is of great environmental importance due to the extreme hazards posed by their presence in small amounts in the ambient. Nitrogen dioxide (NO_2), ozone (O_3), sulfur dioxide (SO_2), particulate matter (PM), carbon monoxide (CO), and lead (Pb) are six principal pollutants of major concern for maintaining the quality of air in urban areas (Table 52.1). Some of these pollutants, like CO, Pb, NO_2, PM, and SO_2, are emitted directly from a variety of sources including industrial production growth and increased traffic congestion. Ozone is generally formed when emissions of NO_2, SO_2, ammonia (NH_3), VOCs, and other gases react in the atmosphere. The presence of ozone in high concentration is also possible in offices where laser printers and photocopiers are heavily used. Conversely, water is commonly treated with O_3 to destroy microbial contaminants such as *Escherichia coli* and *Salmonella* [52.6, 7] and there is a need for accurate calibration of ozone content. Because of its ability to absorb ultraviolet (UV) radiation from sunlight, stratospheric ozone filters out damaging ultraviolet radiation from the sun. Monitoring of ozone in the stratosphere has thus become a global issue as it forms a protective shield for all forms of life on Earth.

Stringent domestic and international standards for emission control require the monitoring of threshold limit values of these pollutants in order to protect primarily against adverse public health hazards. For example, VOCs and nitric oxide (NO_x) resulting from combustion processes cause respiratory problems. Benzene itself is regarded as a human carcinogen and vehicle exhaust is primarily composed of these toxic gases. Spillage in fuel stations also contribute to the emission of excessive amounts of aromatic hydrocarbons in the atmosphere. VOCs also bind with ground-level ozone and form a photochemical smog, causing breathing difficulty for asthma sufferers. The secondary requirement of pollution monitoring is to reduce disastrous effects on the preservation of ecosystems, plants, and animals. Safeguards should also be in place to protect from decreased visibility due to the presence of PM and damage to crops, vegetation, and buildings due to atmospheric pollution. SO_2 content is known to attack buildings both internally and externally, and in particular the surface of historical glasses. A wide variety of preventive conservation tools and routines have been sought to protect historical and cultural objects against deterioration and degradation [52.8, 9].

The activities of chemical sensing are not solely limited to environmental control. Hydrogen (H_2) fuel cells are clean, quiet, more efficient generators of electricity than any other known technology. Hydrogen is also an important raw material for the aerospace, chemical, and semiconductor industries. As hydrogen is explosive above the lower explosive limit (LEL), H_2 sensors have now become important safety devices in all these applications. The oxygen sensor which detects the air-fuel mixture of a gasoline engine by measur-

Table 52.1 Air quality standards for the UK, USA, and World Health Organization (WHO)

Pollutant	UK		WHO		USA	
	Concentration	Standard measured	Concentration	Standard measured	Concentration	Standard measured
Benzene	5 ppb	Annual mean	Data not available			
1,3-Butadiene	1 ppb	Annual mean	Data not available			
Carbon monoxide (CO)	8.6 ppm	8 h mean	8.6 ppm	8 h mean	9 ppm	8 h mean
Lead (Pb)	0.25 $\mu g/m^3$	Annual mean	0.5 $\mu g/m^3$	Annual mean	1.5 $\mu g/m^3$	Quarterly mean
Nitrogen dioxide (NO_2)	21 ppb	Annual mean	105 ppb	1 h mean	0.05 ppm	Annual mean
Ozone (O_3)	50 ppb	8 h mean	60 ppb	8 h mean	0.08 ppm	8 h mean
Particles (PM_{10})	50 $\mu g/m^3$	24 h mean	70 $\mu g/m^3$	24 h mean	50 $\mu g/m^3$	Annual mean
Sulfur dioxide (SO_2)	100 ppb	15 min mean	188 ppb	10 min mean	0.14 ppm	24 h mean

ing the amount of oxygen in the exhaust gas is an essential component of the car engine management system. The development of reliable oxygen sensors for medical application has received considerable research attention in recent years [52.10–12]. Drinking, industrial, and swimming pool water must be disinfected with suitable oxidizing agents such as chlorine or chlorine compounds. The dosing of the appropriate oxidizing agents must be carefully controlled to suit the application as a higher concentration can result in corrosion effects, impairment of taste, or skin irritation. The ability to detect chlorine at sub-ppm level is therefore essential [52.13]. Ammonia is increasingly being used as a refrigerant alternative to ozone-depleting chlorofluorocarbon (CFC). Large quantities of ammonia can also be found in fertilizer factories, resin-production plants using urea, explosive munitions plants, semiconductor industries, and water utility facilities. The presence of ammonia can cause inhalation problems at a very low concentration (0.6–53 ppm). Airborne ammonia gas dissolves in the moisture on the skin, forming corrosive ammonium hydroxide. Exposure to ammonia at 10 000 ppm is mildly irritating to moist skin but the effects become more pronounced with increasing concentration, producing chemical burns with blistering at 30 000 ppm. Its solubility in water can cause it to cauterize respiratory tracts, resulting in deaths at concentrations of 5000 ppm. Research into the development of reliable ammonia sensors with a fast response to a wide range of concentrations is intensive [52.14–16].

It is obvious from the brief survey above that growing demand exists for the fabrication of low-cost, low-power, robust, and portable chemical sensors for a variety of pollutants, contaminants, and analytes, showing improved sensitivity and selectivity for industrial, health care, and environmental control. Analytical chemical tools provide advanced and reliable methods for detection of different analytes but those methods are in many cases prohibitively expensive, unsuited for large-scale field measurements, or mobile monitoring. For instance, there is currently a good market for detection systems for ozone at low concentration (ppb level) to replace more expensive techniques such as UV absorption measurements [52.17]. Existing devices for the detection of ozone are now mostly based on electrochemical measurements [52.18], or on solid-state semiconductor devices [52.19]. Similarly, the detection of organic vapors involves extracting air samples and subsequently analyzing them using standard laboratory techniques such as gas chromatography [52.20], mass spectroscopy, and Fourier-transform infrared (FTIR) spectroscopy [52.21, 22]. The major disadvantages associated with these techniques are their complexity, the capital cost of the instruments used, and the requirement for trained human resources for both operation and the interpretation of data. Apart from environmental applications, the development of detection instrumentation for these species is also important for both human health monitoring [52.23, 24] and for odor detection [52.25].

52.2 Brief Review of Inorganic Materials

Different types of oxide semiconductors have been used for fabrication of gas sensors with a high degree of sensitivity and specificity. The physically interesting electronic and opto-electronic properties of 2D materials have also been exploited over last two decades for environmental and security control.

52.2.1 Oxide Semiconductor Sensors

Solid-state semiconductor gas sensors are usually made of tin oxide (SnO_2) in the form of thick films, porous pellets, or thin-film coatings to monitor the presence of various gases [52.26]. These sensors are being used in the intelligent automatic control of a large number of processes, ranging from microwave cooking to the efficient combustion of motor engines. SnO_2 sensors operate at high temperatures of 300–400 °C. Gases are adsorbed onto the surface in the presence of air and the semiconductivity of the metal oxide changes due to the formation of a surface depletion layer. The thickness of this layer can be expressed in terms of the Debye length $L_D = \sqrt{\varepsilon_0 \varepsilon k_B T/(q^2 n_0)}$, where ε_0 is the permittivity of free space, ε is the dielectric constant of the semiconducting material, n_0 is the total carrier concentration, q is the electronic charge, k_B is the Boltzmann constant, and T is the absolute temperature [52.27]. The sensitivity of the sensor is generally defined as the ratio of the change in conductance after treatment to the conductance of the sensor in air and can simply be written as $\Delta n L_D/n_0$, where Δn is the change in carrier concentration due to analyte exposure. It is therefore possible to optimize the sensitivity by reducing grain size, lowering the carrier concentration, and increasing the Debye length. The maximum sensitivity is assumed to have been achieved when the Debye length is about half the particle size.

Figure 52.1 shows a photograph of a comb-like interdigitated electrode (IDE) system used for most

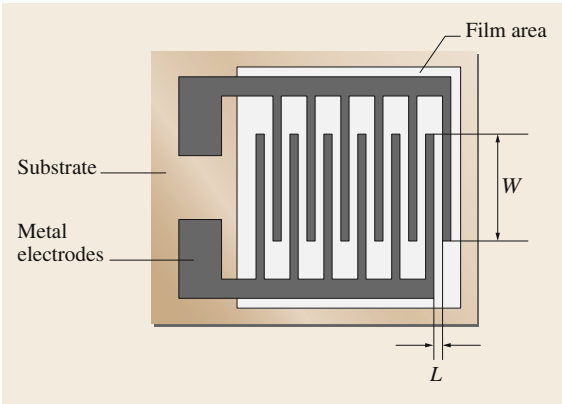

Fig. 52.1 Interdigitated electrode (IDE) system for an SnO_2 sensor

conductivity measurements. The original idea was developed by *Taguchi* [52.28] and the sample resistance in this configuration is smaller than that obtained from the four-contact geometry. The output signal is normally logarithmic to gas concentration. The conductivity change of SnO_2 thick-film sensors was monitored on exposure to compounds forming in smouldering and combustion processes of natural materials, e.g., paper and wood. A strong response was observed for compounds with hydroxyl groups and the highest response was obtained for phenolic structures such as methoxyphenols and benzenediols [52.29]. The response of a SnO_2 sensor element operating at 270 °C produced no sensor response to toluene, furfural, and acetone [52.30]. The impedance output from the SnO_2 sensor array was measured at 300 °C in terms of conductance changes and peak frequency changes. These changes were more sensitive to oxygenated VOCs than other VOCs. The sensor's sensitivity could also be enhanced by using Pd- and Pt-doped sensors [52.31].

Considerable development work is being carried out to integrate the semiconductor sensing membrane with the interrogation and control circuitry on a silicon chip using conventional silicon technology. Using an industrial 0.8 μm complementary metal-oxide-semiconductor (CMOS) process with subsequent micromachining steps, a CO gas-sensor chip was fully integrated with advanced analogue and digital circuitry on a chip for temperature control in the range 170–300 °C with an error of ±2 °C. The whole device was encapsulated using standard microelectronic packaging methods. It was reported that the integrated sensor was capable of measuring CO at the concentration of 5 ppm with a resolution of ±0.1 ppm [52.32].

Solid-state sensor technology relies on the preparation of semiconductor films. SnO_2 sensors suffer from a lack of selectivity and drift. The high temperature required for the surface reactions encourages the growth of grains by coalescence, giving rise to unstable materials. Recent progress in the synthesis of nanomaterials has been employed to overcome some of these problems. Oxide powders were thermally evaporated under controlled conditions without the presence of a catalyst to deposit single-crystalline SnO_2 nanobelts on a platinum IDE structure on an alumina substrate. The surface-to-volume ratio was very high but the size was large enough to contain the depletion layer within the belt. SnO_2 nanobelts were sensitive to CO, NO_2, and ethanol and therefore suitable for applications in breath analysis and food control [52.33].

Advanced methods of information technology are increasingly being used to address the issues regarding selectivity and specificity. A sensor array of two commercial metal-oxide gas sensors was developed to discriminate six organic solvents over a wide concentration range of 2–200 ppm in air. The baseline drift was considerably reduced over a test period of several months by temperature cycling. Further reduction in drift was achieved by suppressing the influence of humidity via additional signal preprocessing. Relatively low computing power was required for the hierarchical pattern classification to evaluate shape features generated from the sensor response curve during temperature cycling. The technique was found to be adaptable to different operating environments, for example, to suppress false alarms from interfering gases [52.34].

Apart from SnO_2, titania (TiO_2), ferric oxide (Fe_2O_3), titania-doped chromium oxide ($Cr_{1.8}Ti_{0.2}O_3$), molybdenum trioxide (MoO_3), tungsten oxide (WO_3), indium oxide (In_2O_3), and perovskite-type thick films ($LaFeO_3$) were studied for sensing a host of analytes such as H_2, CO, NO_2, H_2S, NH_3, and CH_4 in the ppb range. The characteristics of titanium dioxide nanotube hydrogen sensors were found to be completely reversible, highly selective, and free from hysteresis. The sensors showed response times of approximately 150 s at a nominal operating temperature of 180 °C. The sensitivity of the nanotubes was believed to be due to chemisorption of hydrogen onto the titania surface as electron donors. Increased operating temperature improved the sensitivity significantly but reduced the response time. Samples with smaller pore diameter (46 nm) were more sensitive to hydrogen than those with larger pore diameter (76 nm). The sensor showed a response to high concentrations of oxygen but the response time was long and the recovery was not complete [52.35]. Ion-beam-deposited thin films of MoO_3 on alumina substrates with gold IDEs showed selective response to NH_3 at 450 °C. Similarly prepared WO_3 thin-film samples were highly sensitive to NO_2. Both films exhibited orthorhombic structure but the polymor-

phic dissimilarities between two types of materials were responsible for the difference in their sensing behavior [52.36].

52.2.2 Graphene Based Sensors

Successful mechanical exfoliation of a highly oriented pyrolytic graphite sample to produce thin layers of graphene was reported in 2004. A one-atom-thick single layer of graphene consists of sp^2-hybridized carbon atoms arranged in a hexagonal lattice. The overlap between the conduction and valence bands is found to occur in ambilar monocrystalline thin films showing a large carrier concentration of $10^{17}\,cm^{-2}$ and high mobility up to $10\,000\,cm^2V^{-1}s^{-1}$ [52.37]. Mechanical exfoliation, sonication-assisted liquid exfoliation, and chemical vapor deposition (CVD) are commonly used to synthesize high-quality graphene films with a reduced number of defects by annealing. However, these methods are not suitable for deposition over large areas. Printing can be used as an alternative technique to make conductive graphene films. Some of the advantages of graphene printing are the low processing temperature under ambient conditions without using a vacuum or inert atmosphere. The other benefit of graphene printing is that films can be obtained over large areas on flexible substrates, at a reduced cost. Figure 52.2 shows the scanning electron microscopic (SEM) image of a drop-cast film of graphene. The graphene ink was formulated with few-layer graphene particles of lateral dimensions $< 40\,\mu m$, which were obtained by liquid-phase exfoliation. The graphene particles were dispersed in an acrylic polymer system to obtain the ink suitable for thin-film deposition on flexible substrates. The sample consisted of a disordered layered structure with a single isolated graphene flake as shown in the inset.

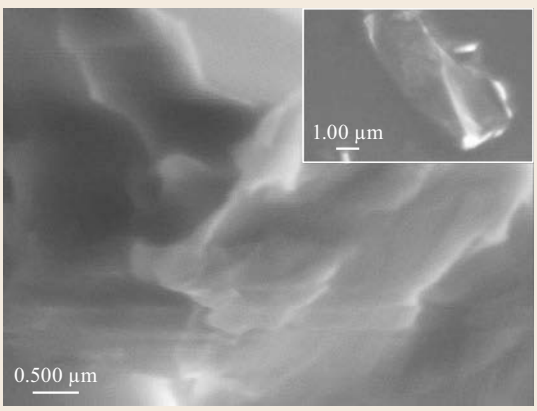

Fig. 52.2 Scanning electron microscopic image of a graphene ink sample drop cast onto aluminum foil

Considerable research efforts have been spent over the last two years to exploit the unique optoelectronic properties of these highly π-conjugated two-dimensional (2-D) materials for the development of a variety of sensors with potential applications in security, environmental and safety control, and disease detection and diagnosis [52.38]. Intrinsic graphene is found to be highly sensitive in detecting industrial toxic gases such as CO, NO_x, and NH_3, but selectivity is poor for practical applications. Considerable improvement in selectivity can be achieved using hybrid structures of graphene blended with metal oxide nanoparticles [52.39]. The electrochemical potential window of 2.5 V for the graphene electrode in 0.1 M phosphate-buffered saline with a pH value of 7.0 is very comparable to those obtained for glassy carbon (GC) and boron-doped diamond. Also, AC impedance measured graphene charge-transfer resistance is smaller than their competitive electrodes. These superior electrochemical properties of graphene have been exploited in recent years to develop the oxidase sensors for detecting the presence of hydrogen peroxide H_2O_2 in food, pharmaceutical, clinical, industrial and environmental analyses with a high degree of reliability and sensitivity [52.40]. The presence of heavy metals such as lead (Pb^{2+}), cadmium (Cd^{2+}), chromium (Cr^{3+}, Cr^{6+}), mercury (Hg^{2+}), copper (Cu^{2+}), and arsenic (As^{3+}) ions in atmosphere and water is recognized by the World Health Organization as a severe threat to human health. Field-effect transistors (FET) using protein-functionalized reduced graphene oxide (RGO) films as an active channel have been employed to record the change in transconductance due to the contamination of target metal atoms. A value of $2.5\times10^{-8}\,mol\,l^{-1}$ for the detection limit and a faster response time of less than 10 s were observed in Hg^{2+} monitoring with thermally reduced GO film decorated with thioglycolic-acid-functionalized gold nanoparticles (AuNps) in an active FET channel. These FET sensors are portable and cost-effective compared to turn-on fluorescence sensors based upon fluorescence resonance energy transfer. It is, however, reported that fluorescence based upon hybrid graphene-gold nanoparticles (AuNp) is able to detect Pb^{2+} ions selectively up to the limit of $10^{-8}\,mol\,L^{-1}$ over the common metal pollutants in an aqueous solution. This effect is attributed to accelerated leaching of AuNp by Pb^{2+} ions. The highly hydrophobic surface with a large specific surface area in the order of $2600\,m^2g^{-1}$ makes graphene very suitable for adsorbing aromatic organic pollutants in water [52.41]. Cofactors such as nicotinamide adenine dinucleotide hydrogen (NADH) are catalytic agents for many important biological activities in the human body. During mitochondrial respiration, the electron transfer takes place

through the NADH producing sufficient adenosine triphosphate (ATP) enzymes for cellular energy supply. The concentration of NADH varies in different parts of the body depending on the energy requirements. An unexpected elevation or lowering of NADH may cause severe diseases like brain ischaemia and Leigh syndrome. The oxidation of the NADH serves as the anodic signal and regenerates the NAD^+ cofactor. The shift of peak potentials of NADH oxidation from 0.70 V on the GC to 0.40 V on the RGO electrode makes graphene a suitable material for highly sensitive electrochemical biosensors of low working potentials, offering low detection limits and long-term stabilities [52.42]. Graphene oxide (GO) and its reduced form (RGO) are studied extensively in the field of biotechnology because of their multivalent functionalization and efficient surface loading with various biomolecules. The negative surface charge originating from a free π-electron cloud can be utilized to condense genes and anticancer drugs. For example, when 6-armed polyethylene glycol (PEG) was covalently linked to the surface of GO sheets to form biocompatible GO-PEG, which is nontoxic to human lung and breast cancer cells. Graphene may act as a potential antimicrobial coating for surgical equipment by preventing the formation of pathogenic and corrosive microorganisms and even killing bacteria. Real-time high-resolution optical imaging as well as electrophysiological recording of neuronal locations are essential for examining the operation of individual neural circuits in neurological disorders. As conventional metallic microelectrodes are opaque, they shadow the investigator's view, making it necessary to record the imaging and electrophysiological data separately. However, transparent, flexible graphene electrodes may now be used for the simultaneous temporal and spatial resolution required for neuroscientific treatments. The nonmagnetic and anti-corrosive properties of graphene offer added advantages [52.43].

52.3 Macrocylic Compounds for Sensing

Phthalocyanine molecules belong to a class of macrocylic compounds. Because of their 18 π-electron aromatic macrocyclic structure these molecules exhibit important optoelectronic, photophysical, conduction, and photoconduction properties [52.44]. As shown in Fig. 52.3, the Pc structure is closely related to the naturally occurring porphyrins, which form a core skeleton in hemoglobin and chlorophyll. Organic molecular nanostructures have huge potential but suffer from unstable device characteristics, low resistance to adverse environments (e.g., temperature, humidity, oxygen, etc.) and lack of reproducibility of material composition, purity, and fabrication conditions. Phthalocyanines (Pcs) are, however, tinctorially strong, and chemically and thermally stable. The materials are abundantly available in a highly purified form.

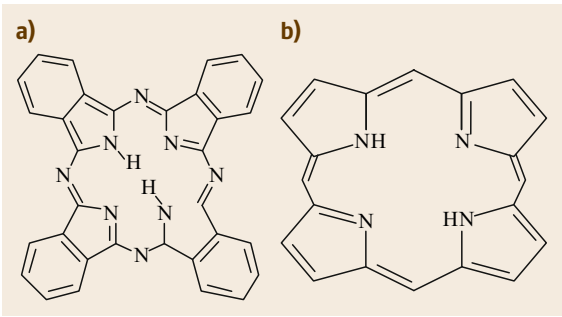

Fig. 52.3a,b Chemical structure of: **(a)** a metal-free phthalocyanine and **(b)** porphyrin molecule

52.3.1 Preparation of Sensing Membranes

Sensing is essentially an interaction mechanism of a solid surface and analytes and the molecules are organized in ultrathin films, offering a large surface-to-volume ratio to improve the probability of these reactions taking place. A variety of methods such as direct-current DC and radio-frequency RF sputtering [52.45], thermal evaporation [52.46], Langmuir–Blodgett (LB) [52.47], spin coating [52.48], and self-assembly (SA) [52.49] are employed to produce organized thin organic films.

The substrates play a key role in determining the film quality and the structure. It is found that the island density and coverage ratio of copper tetra-*tert*-butyl phthalocyanine (CuTTBPc) on hydrophilic glass surfaces were small during the early growth stage of vacuum deposition due to a small nucleation rate arising from the weak interaction of molecules. The film surface was also rough. The high nucleation rate of CuTTBPc on a silanized surface, on the contrary, produced a much smoother morphology consisting of densely distributed fine-grained clusters. The aggregation of the molecules took place in domains during the formation of the LB monolayer, separately distributed on the glass surface. These domains acted as active sites for the nucleation and growth of the later deposition process and high-density clusters were thus found in the early growth stage. X-ray diffraction (XRD) patterns demonstrated

that the LB films grown on the glass substrate were more crystalline than those on other substrates [52.50].

The wet techniques, namely LB, spin coating and SA, are preferred to high-energy deposition because the deposition takes place at room temperature, reducing the possibility of chemical decomposition of the molecules due to thermal damage. These deposition methods are considered below.

Langmuir–Blodgett (LB) Technique

The LB method involves the transfer of individual Langmuir monolayers of amphiphilic molecules which self-assemble in an ultra-clean water subphase onto a suitably prepared solid substrate. An LB film, which may consist of a single or many layers, up to a depth of several visible-light wavelengths, is generally produced with fine control over the thickness and geometry to a precision at the molecular level. With the Y-type construction, these LB films are essentially layered materials with alternating hydrophobic/hydrophillic regions. Noncentrosymmetric LB films can be obtained by X-type construction on immersion of the substrate from air into water only, or Z-type deposition on withdrawal of the substrate from water to air [52.51].

Macrocylic molecules are not generally amphiphilic and are therefore not considered suitable for LB deposition. The synthesis of a series of specially designed Pc molecules for LB deposition has been reported in the literature over the last two decades [52.52–54]. Figure 52.4 shows the chemical structure of asymmetrically substituted 1,4-bis(6-hydroxyhexyl)-8,11,15,18,22,25-hexa-octylphthalocyanine molecules belonging to this family of custom-designed molecules [52.55].

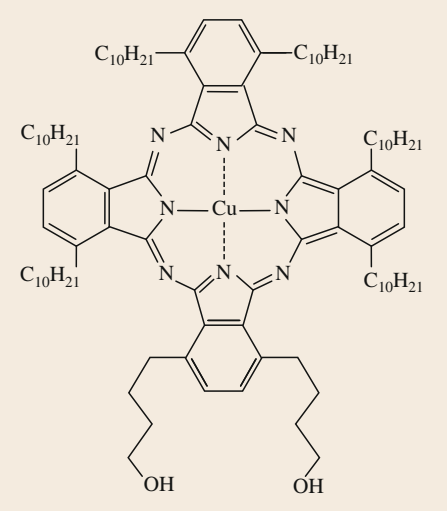

Fig. 52.4 Chemical structure of 1,4-bis(4-hydroxybutyl)-8,11,15,18,22,25-hexakisdecyl phthalocyaninato copper molecules

To start with LB deposition, a Langmuir monolayer is formed from a spreading solution of substituted Pc derivatives in an appropriate volatile solvent (such as chloroform) on the highly purified water subphase (Milli-Q water of resistivity 0.18 MΩm) contained in an LB trough made of a hydrophobic material (Teflon). The solvent is allowed to evaporate fully and the molecules are then slowly compressed to the desired organization by closing a servo-controlled Teflon barrier straddling the air–water interface at a constant speed (say about 100 mm/min). As shown in Fig. 52.5, the phase changes of the molecules during the compression are monitored by recording the surface pressure–area isotherm. The pressure begins to rise rapidly as the solid phase is reached while the area per molecule remains approximately constant. The molecules are transferred from the water–air interface to the substrate by dipping the substrate in at a constant speed of about 10 mm/min when the surface pressure is

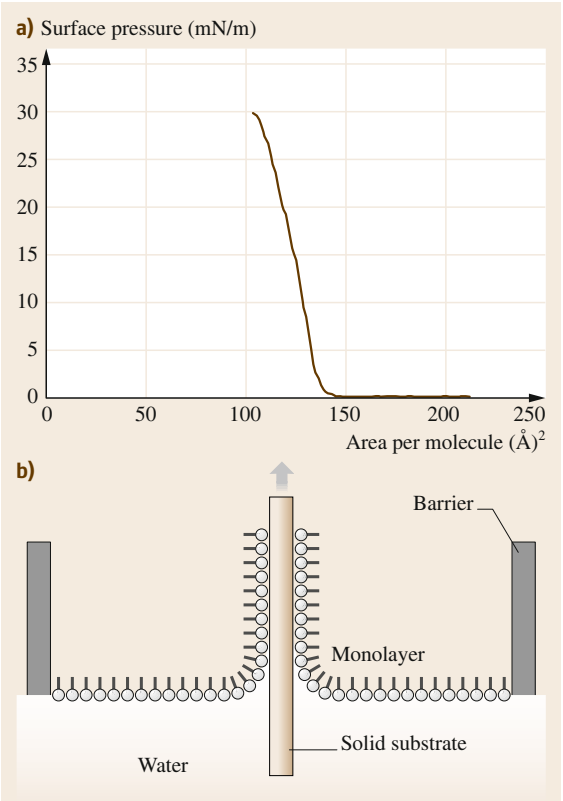

Fig. 52.5a,b Deposition of Langmuir–Blodgett film: **(a)** surface pressure–area isotherms and **(b)** transfer of floating monolayer onto a suitable substrate floating monolayer

in the range 20–40 mNm^{-1}. However, a dipping rate as high as 1000 mm/min was used to produce LB films of 5,10,15,20-tetrakis(3,4-bis[2-ethylhexyloxyphenyl])-21*H*,23*H*-porphine (EHO) molecules. Atomic force microscopy (AFM) showed a morphology of these films which is highly conducive to the host–guest interaction. The presence of isolated micron-sized domains, which were themselves composed of grains of several nm in diameter, was observed [52.56].

The molecular orientation in LB films of these novel substituted Pc derivatives was investigated by spectroscopic methods, including electron spin resonance, reflection adsorption infrared spectroscopy (RAIRS), polarized infrared (IR) spectroscopy, and AFM. Amphiphilic mesogenic Pcs afforded the best films. These all contained a good degree of molecular order. Furthermore, the type of molecular stacking in the films was found to depend upon the length of the side chains and the central metal [52.57].

Spin-Coating Method

The spin-coating method, designed for defining patterns on silicon wafers in integrated circuit (IC) technology, has now been adapted for deposition of thin organic films on suitable substrates [52.58]. Substrates are vacuum held onto the rotating chuck of a photoresist spinner. The spread solution was prepared in the same way as done for the LB deposition and a small volume of the solution is dispensed onto the rotating substrate surface from a microsyringe held at a distance of 5 mm above the spinner platform. A spinning time of 30 s for a solution concentration of 0.5–5.0 mg/ml is found to be sufficient in order to produce a uniform, homogeneous film. The rotation speed is normally varied between 1000–6000 rpm and the speed of spin and the concentration of solution largely determine the thickness of the resulting films. The dependence of the film thickness d on spin speed ω and time t may be written in terms of an empirical expression [52.59]

$$d = \frac{C}{\sqrt{t}}\omega^{-x}\,, \tag{52.1}$$

where C depends upon the evaporation rate of the solvent, and the viscosity and density of the solution. The index x is predominantly determined by the evaporation rate of the solvent. If the evaporation of the solvent is independent of the spin speed, x takes on a value of $2/3$. For most solvents used, the evaporation varies with $\sqrt{\omega}$ and x becomes $1/2$. A value of $x = 1$ is a valid approximation for slow evaporation [52.60, 61].

Spin coating is a simpler and more cost-effective method than LB deposition and also there is no requirement for the molecules to be amphiphilic. The LB technique, however, provides more precise control over the film thickness [52.62]. Both spun and LB thin films of octa-alkyl-substituted phthalocyanine molecules displayed similar characteristic features in their optical absorption spectra. The appearance of Davydov splitting and the XRD pattern indicated the same crystallinity of the films [52.63]. Different physical structure and molecular packing may result from the use of different wet techniques. For instance, asymmetrically substituted phthalocyanine molecules (Fig. 52.4) were deposited by LB and spin-coating techniques. XRD patterns and UV-Vis spectra of these films indicated some degree of anisotropic ordering within the LB films compared to spun films [52.64]. The spin-coated films were, however, exceptionally smooth, even and free from crystallites. A noncompact spin-coated film of phthalocyanine molecules bearing one crown on the ether ring exhibited a faster response and reversal time than the well-ordered and tightly packed LB films [52.65].

Self-Assembled Monolayers (SAMs)

Self-assembled monolayers (SAMs) have attracted considerable interest because of their simplicity of preparation, stability, and versatility. The introduction of due functional groups into SAMs allows changes of state and property on surface or interface. These attributes make SAM films attractive for sensor technology [52.66, 67]. SAM films are formed via reaction of a functional group within a molecule with the surface of a solid substrate. The methoxy or trichlorosilylalkyl derivatives of molecules form weak bonds with hydroxyl groups and are suitable for the formation of a SAM on an oxide surface such as indium tin-oxide (ITO) and glass (SiO_2) [52.68]. A monolayer layer can also be self-assembled on gold or silver substrates if the molecules are attached with thio or disulfide groups at one end [52.69]. In supramolecular aggregation during the self-assembly process, the interactions between the adsorbate molecules are as important as those between adsorbates and the surface. The size and aggregation pattern for the formation of supramolecular structures (J-aggregates) are controlled by changing the number of polar sulfonic groups of meso-tetra (4-sulfonatophenyl) porphine [52.70].

Much fundamental work on SAM films was initially undertaken with simple functionalized alkane derivatives [52.71]. In the case of alkylthiols on gold, it is well established that the monolayer films were densely packed with a high degree of order, with chains typically oriented at about 65° to the substrate surface. In recent years, work has been undertaken to include a single tether chain with thiol or disulfide derivatives for SAM formation on gold-coated glass substrates.

The molecular orientation with respect to the gold surface was found to depend upon the different alkyl-connecting chain lengths and different macrocyclic peripheral side chains [52.72]. The core of substituted Pc molecules bearing mercaptoalkyl groups is not parallel to the surface if the tether chain is increasingly long. For sufficiently long tethers, the core becomes oriented almost normal to the surface [52.73]. SAM films of thiol-derivatized cobalt phthalocyanine complexes on gold electrodes were susceptible to destruction via oxidative and reductive desorption and their potential applications as a sensor were therefore limited [52.74].

Self-assembled ultrathin films have recently received considerable interest because they allow fabrication of supramolecular assemblies with tailored architecture and properties [52.75]. Multilayered films can also be built up by sequential deposition of polycations and polyanions based upon electrostatic attraction [52.76–78]. Alternate deposition of planar functional molecules meso-tetra (4-sulfonyl) porphyrin ($TPPS_4$) or copper phthalocyaninetetrasulfonic acid, tetrasodium salt (CuTsPc) and cationic bis (pyridinium) salt was made to produce a self-assembled multilayered film [52.79]. Multilayer assemblies of porphyrin and phthalocyanine were also prepared by alternating deposition of oppositely charged rigid planar molecules of sodium (phthalocyanine tetra-sulfonate)cobalt $Na_4[(CoTsPc)]$ and tetrakis(N,N,N-trimethyl-4-anilinium) porphyrin cobalt $[(CoTAP)]Br_4$ [52.80]. A further investigation of the C-11 Pc derivative SAM has shown that the monolayer film was stable, exhibiting no oxidation and only minor orientation changes on the gold surface over a period of 24 months as determined by infrared and fluorescence spectroscopy. The long active life of the Pc SAM was thought to be due to the macrocyclic ring possibly preventing oxidation of the thiolate root [52.81].

52.3.2 Thin-Film Properties

Surface/interface composition at the nanometer scale is believed to affect the organization and chemical/physical properties of organic thin films. This long-range organization determines both the optical and electrical properties of thin-film materials, leading to unique, new chemical sensor platforms. The overlap of π-electron wave functions from Pc molecule to Pc molecule is likely to occur between adjacent stacks in a thin-film form, giving rise to the broadening of energy levels [52.82].

Phthalocyanine Films

Phthalocyanines can exist in different polymorphic forms: α and β are among the most common. Both forms possess the herringbone structure for the stacking arrangement. The angle between the stacking axis and the normal to the molecular plane depends upon the method of preparation, types of phthalocyanine (metallo or metal-free), and substituents. For example, this angle is generally 25° and 45° for the α and β phases, respectively [52.83]. A typical absorption spectrum in the UV-visible range is shown in Fig. 52.6 for a substituted metal-free phthalocyanine (Pc) deposited on a glass substrate (similar to one shown in Fig. 52.3). The Q absorption band of the LB film was broader than one for the chloroform solution and appeared at wavelengths between 650–800 nm. The Davydov splitting became apparent when compared with the spectra for the molecules in chloroform. The film-forming properties and the stack order were both found to be influenced by the chain length of the ring substituents [52.84, 85]. An analysis into the in-plane molecular arrangements in the LB films of Pc compounds with short and long alkyl chains was performed by decomposing the absorption spectra into Gaussian–Lorentzian components. Long-chain molecules were found to be organized in a *herringbone* structure leading to the Davydov splitting of the Q-band. For short-chain molecules, the largely broadened blue component of the Davydov doublets was suppressed possibly due to the domination of an anisotropic stack-like molecular arrangement in LB films [52.86]. Characteristic Q-bands observed at about 630 nm in the UV-Vis spectra of the self-assembling monolayers (SAMs) of 2,9,16-tri(*tert*-butyl)-23-(10-mercaptodecyloxy)phthalocyanine and its disulfide on gold substrates were broadened and blue-shifted relative to those observed in solution [52.87]. The formation of high-quality Langmuir–Blodgett films of copper (CuPc) and nickel phthalocyanine (NiPc) derivatives

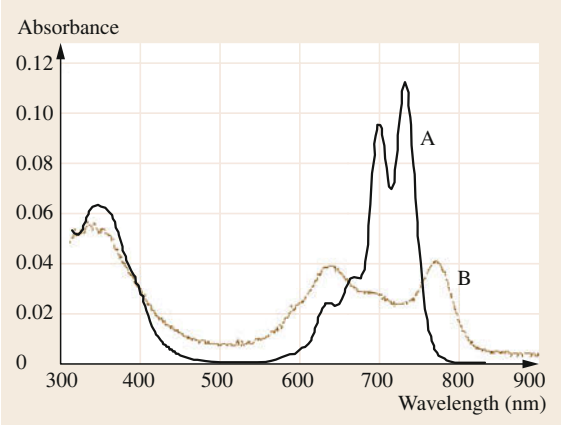

Fig. 52.6 Typical UV-visible spectra for thin films of metal-free phthalocyanine molecules in: (A) chloroform and (B) an LB film

substituted with short branched chains is reported. Ellipsometric and polarized optical absorption measurements suggest that the phthalocyanine molecules have a preferred orientation, with their large faces perpendicular to the dipping direction and to the substrate plane [52.88].

Electrical properties of Pc molecules are very dependent upon the doping and the nature of the substituents in the macrocyclic compounds. Copper(II) tetrasubstituted phthalocyanine complexes, CuPcX (where X = $-NO_2$, $-NH_2$, $-SO_3H$, and $-OH$) exhibited an improvement of conductivity by five orders of magnitude over its unsubstituted counterpart. Further enhancement in conductivity was achieved by iodine doping. This increase in conductivity was attributed to the possible decrease in the metal–metal bond distance [52.89]. The effect of oxygen on charge transport was investigated by measuring the time-dependence behavior of the film conductivity of zinc Pc (ZnPc) layers at a stable pressure of about 0.1 mbar of air and it was found that the conductivity gradually decreased by an order of magnitude with time. The conductivity reached saturation within several minutes for the film thickness smaller than 500 nm whereas similar electrical degradation in a 7 μm-thick film required more than half an hour. This thickness-dependent decrease in conductivity was caused by the velocity of the oxygen out-diffusion processes in the films [52.90]. The effect of doping on conductivity of a thermally deposited composite film of α-nickel phthalocyanine (NiPc) and the strong electron acceptor tetracyanoquinodimethane (TCNQ) was investigated by exposure to air. The doping took place at a much faster rate in the composite than in the NiPc films. Values of 1.3 and 1.9 eV for the activation energy were obtained for devices incorporating TCNQ and the non-TCNQ devices, respectively, and the conductivity of the composite film was therefore found to be 20 times larger than the NiPc film [52.91]. Because of the excellent ability to photogenerate free charge carriers, the conductivity of the metal phthalocyanine (MPc) film is increased considerably as can be seen in Fig. 52.7 showing the dark and illuminated current–voltage characteristics of a 10 nm-thick spun nickel phthalocyanine (NiPc) sandwiched between two metal electrodes.

Phthalocyanines of rare-earth metals primarily occur in the form of bisphthalocyanines with a sandwich-type structure and the cation is eightfold coordinated to the two macrocycles. One of these phthalocyanine rings is virtually planar while the other is significantly distorted [52.92]. The Q-band in the absorption spectra of spun films of substituted lutetium bisphthalocyanine molecules becomes broader and red-shifted compared to the molecules in chloroform solution. Heat treatment of the film at temperatures above 120 °C introduced molecular ordering, possibly due to the edge-to-edge interaction between neighboring Pc moieties [52.93]. All these factors have led to successful formulation of phthalocyanines as chemically sensitive membranes for environmental monitoring [52.94–98].

Porphyrin Films

Inherent stability, unique optical properties, and synthetic versatility of porphyrins and metalloporphyrins are exploited in sensor applications. Synthetic porphyrins and metalloporphyrins incorporated into polymers, glasses, and Langmuir–Blodgett films matrices are used for detection of NO, CO_2, and O_2 because of the ability to bind these gases. Metalloporphyrin sensing arrays have been used for the detection of organic odorants, such as amines, thiols, and phosphines [52.99]. Porphyrins also combine readily with metals, coordinating with them in the central cavity. Many gas sensors take advantage of analyte binding to the center metal atom in the porphyrin ring and a detectable optical change occurs as a result. In particular sensing properties of iron, zinc, copper, nickel, and cobalt containing porphyrins have now been studied [52.100–103]. The porphyrin rings of thiol-derivatized cobalt(II)-5,10,15,20-tetrakis(4-*tert*-butylphenyl)-porphyrin (CoTBPP) molecules were immobilized on the surface of a 4-aminothiophenol (4-ATP) self-assembled monolayer (SAM) on gold (111) by in situ axial legation. The reconstruction of the herringbone structure took place probably due to adsorption/desorption processes of molecules [52.104].

Substituents have considerable effects on the structure of porphyrin monolayers; for example, the interaction between the porphyrins deposited on the ITO

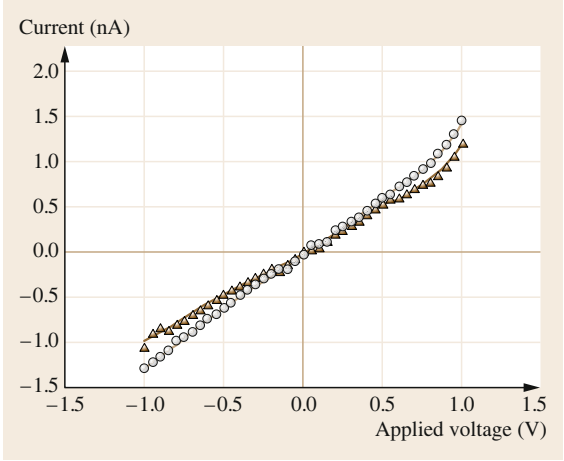

Fig. 52.7 Dark- (*triangles*) and photoconduction (*circles*) through spun NiPc films

substrate without bulky *tert*-butyl groups was much stronger than that of the porphyrins with bulky *tert*-butyl groups [52.105]. Hybrid molecule-silicon capacitors were formed by attaching [5-(4-dihydroxyphosphorylphenyl)-10,15,20-trimesitylporphinatozinc(II)] porphyrin complexes to silicon oxide via a phosphonate linkage and the presence of multiple distinct peaks in electrical characteristics were associated with oxidation and reduction of the molecular monolayer [52.106]. Multilayered thin films of porphyrins bearing bulky alkoxyphenyl substituents at two of the four meso-positions and phenyl phosphonates at the other two were deposited on the ITO substrates using the zirconium phosphonate linkage. Molecular aggregation was prevented by the addition of sterically demanding 2,6-di(*n*-hexoxy)phenyl substituents to the meso-positions of the porphyrin skeleton. The compounds were able to form thin films without the presence of large molecular chromophore interaction relative to sterically unhindered porphyrins [52.107]. Highly conducting tetraruthenated cobaltporphyrin (Co (TRP)) and tetrasulfonated zincporphyrin (Zn (TPPS)) multi-bilayer films were prepared by electrostatic assembly for sensor applications [52.108].

52.4 Sensing with Phthalocyanine and Porphyrin

The interaction of reactive gases such as O_2, NO_2 and NH_3 with the phthalocyanine group of compounds has been shown to result in conductivity changes of these compounds. This effect was associated with charge transfer between the electron-donating phthalocyanine molecule and the electron-accepting gas [52.109].

52.4.1 Amperometric Sensor

The action of the oxidizing gases O_2 and NO_2 and the reducing gases NH_3 and H_2 diluted in N_2 on the electrical conductivity of thin layers of zinc hexadecafluorophthalocyanine ($ZnF_{16}Pc$) and zinc phthalocyanine (ZnPc) was investigated. The conductivity $ZnF_{16}Pc$ increased in the presence of NH_3 whereas ZnPc exhibits no sensitivity to this gas. The sensitivity to H_2 was higher for $ZnF_{16}Pc$ than for ZnPc. This behavior was related to the redox potentials of the two phthalocyanines [52.110, 111].

Response and recovery times for LB CuTTBPc films on platinum IDE are shown in Fig. 52.8 for different gas concentrations of 1–5 ppm. These times were determined from a model based upon the kinematics of adsorption and desorption of NO_2 gas molecules. It was found that recovery times were longer than response times, irrespective of gas concentration. The response time constant varied in the range 105–159 s. Repeated exposures to NO_2-air mixtures resulted in gradual degradation of reproducibility. The response was also believed to be influenced by the past history of the exposure of the sensor to the NO_2 gas, if the recovery time constant was longer than the switch-off time. These factors show that CuTBPc is a material that is suitable for fabricating a disposable *single-shot* NO_2 sensor for practical uses [52.112]. LB films of asymmetrically substituted phthalocyanine, 1,4-bis (4-hydroxybutyl) 8,11,15,18,22,25-hexaoctylphthalocyanine molecules showed selective responses to 1–5 ppm concentrations of NO_2 at the room temperature. Moisture had no effect on the response because of the hydrophobic nature of the alkyl groups. Exposure to Cl_2, NH_3, SO_2, and CO at ppm levels produced no measurable response [52.113]. Further work on the LB films showed that the NO_2 response was larger for the LB film produced by dipping the substrate perpendicular to the electrode finger than those dipped parallel to the fingers. This preferential behavior was attributed to the ease of conduction along the long chains [52.114]. LB films of meso,meso′-buta-1,3-diyne-bridged Cu(II) octaethylporphyrin dimer molecules were used to fabricate amperometric sensors operating at a temperature of 90 °C. LB multilayers were reported to be selectively sensitive to small concentrations of NO in air without being affected by contemporary presence in NO_2, CH_4, C_2H_5OH, and CO [52.115].

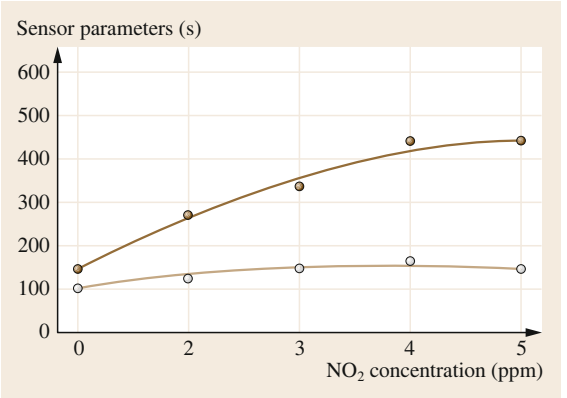

Fig. 52.8 Response (*broken line*) and recovery (*solid line*) of a 15-layer LB film of CuTTBPc when exposed to NO_2 periodically at 2 min intervals at 1, 2, 3, 4, and 5 ppm levels in succession

Thickness, operating temperature, doping and postdeposition treatment of sensing membranes all affect sensor performance. Vacuum-deposited CuPc of thickness 50–400 nm onto gold IDEs on glass substrate were exposed to NO_2 gas of concentration 10–100 ppm. The film thickness had little effect on room-temperature sensitivity, but the recovery ratio decreased with increasing film thickness. Thicker films showed improved recovery at 100 °C [52.116]. Because of the tetra-*tert*-butyl substitution on the periphery of phthalocyanine, CuTTBPc films have a larger lattice spacing and higher film resistance. Sublimed CuTTBPc film showed a higher recovery ratio in the NO_2 sensing experiments [52.117].

NO_2 and O_2 treatment of evaporated CuPc films that were 160–200 nm thick on IDE improved the sensitivity and recovery time when exposed to 0.5–5 ppm of NO_2 gas. A Langmuir behavior was predicted for the adsorption/desorption processes on the weakly binding surface sites of NO_2-treated CuPc films having a single activation energy [52.118]. When the CuPc films were subjected to postdeposition treatment by cooling down to 77 K, the mechanism of NO_2 adsorption, however, followed the Elovich model [52.119]. CuPc and iron Pc (FePc) films (100 nm thick) were heat treated at 240 °C under vacuum and then the responses of the films to the exposure of NO_2 in the 8–12.8 ppm range were monitored. The CuPc films were transformed to a stable β-phase and the adsorption occurred on the ligand rings. Conversely, NO_2 was adsorbed on both the ligand ring and the central ion of the FePc films [52.120]. An amperometric sensor was fabricated using the spun film of tetra-*iso*-propoxyphthalocyaninato copper(II) (*i*-Pro-CuPc), and the response, recovery, and cyclic properties of the sensor were very temperature sensitive. The results showed ideal gas sensitivity at 65 °C and a good linear relationship existed between the resistance of the gas sensor and the concentration of NO_2 [52.121]. NiPc films (25 nm thick) were deposited between the source and the drain of a field-effect transistor (FET) and the change in the drain current exhibited a linear dependence on the ozone concentration in air, in the range 0–150 ppb [52.122, 123].

Water-soluble copper phthalocyanine tetrasulfonate (CuTsPc) molecules were alternatively self-assembled with a bipolar pyridine salt on a 3-mercaptopropionic-acid-modified Au electrode to produce copper ion-selective electrodes (ISE). These ISE were found to have low resistance, short conditioning time, and a fast response. The electrode potentiometric response showed a selective potentiometric response to Cu^{2+} ions in the range from 10^{-5}–10^{-1} M, independent of the pH of the solution between pH 1–5. The response was dependent on the nature of the medium and the detection limit was found to be 7×10^{-6} M in acetate buffer (0.2 M, pH 4.5) [52.124]. Carbohydrates were detected by flow-injection analysis at the water-soluble cobalt phthalocyanine tetrasulfonate (CoTsPc)-modified electrode with high sensitivity. Detection limits obtained in this manner range from 150 pmol injected for glucose and fructose to 600 pmol injected for maltose and sucrose [52.125].

52.4.2 Optical Sensors

The amperometric approach generally suffers from long response times and their use is restricted due to possible fire and explosion hazards caused by electrical power. Organic systems are also prone to slow degradation arising from the chemical reactivity of charge carriers. Conversely, optical transduction techniques offer high speed, high precision, immunity to interference, and remote sensing capabilities for detection of trace gas species.

Optical Absorption and Fluorescence Spectra

Optical transmittance of thermally evaporated lead phthalocyanine (PbPc) and nickel phthalocyanine (NiPc) thin films changed on exposure to NO_2 in the IR region of the optical absorption spectrum [52.126]. The disappearance of Davydov splitting from the UV-Vis absorption spectra of 20-layer-thick LB films of 1,4-bis(4-hydroxybutyl)-8,11,15,18,22,25-hexakisdecyl phthalocyaninato copper molecules was observed when the films were exposed to 100 ppm of NO_2 [52.127]. The local interaction between the central metal atoms and NO_2 distorted the herringbone structure. Gas adsorption and desorption processes were described by exponential functions, both characterized by a single time constant. The dispersion relation in Fig. 52.9 for the refractive index was obtained by using the simple Kronig–Krammer transform of absorption spectra of the LB thin film of another octasubstituted metal-free phthalocyanine molecule. The full recovery of the refractive index to its original value was achieved after flushing with the N_2 gas for wavelengths larger than 782 nm. Ellipsometry measurements on thin films of tetrasulfonated copper phthalocyanine showed increases in the real and the imaginary parts of the dielectric constant on exposure to NO_2 gas possibly due to the rise in the density of dipoles and higher absorption, respectively [52.128].

LB films of 5,15-bis(4-aminophenyl)-10,20-bis[3,4-bis(2-ethylhexyloxy)phenyl]-21H,23H-porphine prepared at a dipping rate as high as 500 mm/min showed an inhomogeneous structure with high porosity. These porphyrin films showed much faster response to 4.6 ppm of NO_2 gas and a sensitivity of 60% relative to absorbance change at 439 nm was achieved.

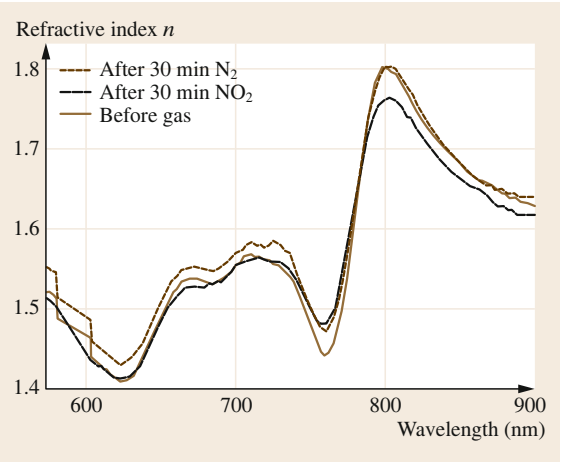

Fig. 52.9 The dependence of the refractive index of octa-substituted phthalocyanine on the wavelength before and after exposure to 90 ppm NO_2 gas for 30 min. The recovery was examined after flushing of the LB films with N_2 for 30 min

Full and accelerated recovery of the original spectrum was also achieved by gentle heating at 353 K. The sensor was reported to have a shelf-life as long as one year [52.129]. Kinetic UV-Vis spectroscopic measurements were made on a porphyrin-entrapped sol–gel film for NO_2 sensing. The method was capable of detecting levels as low as 176 ppb of NO_2 at room temperature and showed a fast and full recovery [52.130]

The blue color of rhodium phthalocyanine LB films becomes transparent upon chlorination. A pronounced quenching of the characteristic triplet centered on the Q-absorption band took place at 662 nm, but the absorption band in the near UV part of the spectrum remained almost unaffected. Optical spectra partially recovered when the exposed film was left in air for several hours. Overall effects of chlorination (quenching and recovery) depended on the period of exposure [52.131]. LB gadolinium phthalocyanine films were exposed to 10 ppm of chlorine and changes in optical absorption spectra were observed as a result of the oxidation of the film by chlorine to form $[Gd(Pc)_2]^+$ species. The kinetics of such changes were described by a polyfunctional process with different decay time constants and the effects were found to be highly reversible [52.132].

SAM films are of interest because the chemically bound monolayer is intrinsically more robust than LB films and the response times are also expected to be faster. Monolayers of diphthalocyanine disulfide Pc molecules were self-assembled on gold-coated glass substrates with the Pc macrocycle oriented parallel to the metal surface. Changes of the reflectivity signal were observed on exposure to NO_2 gas in proportion to the concentration [52.133]. The fluorescence emission spectrum of each of the Pc SAMs was obtained by exciting each monolayer along the longitudinal axis of the optical waveguide via laser-induced evanescent-wave stimulation. The use of the longer mercaptoalkyl connecting chain appeared to inhibit quenching of the electronically excited state through energy transfer to the metal layer. Fluorescence response to 10 ppm NO_2 was found to be selective with no interference from CO and CO_2 [52.134].

Surface Plasmon Resonance Technique

The surface plasmon resonance (SPR) technique is based on the excitation of surface electromagnetic waves of transverse magnetic (TM) modes traveling along the interface between a metal and a dielectric medium. Using a semicylindrical prism of high refractive index n_p in *Kretschmann*'s configuration, as shown in Fig. 52.10, these waves are excited by a p-polarized light of wavelength λ via the evanescent field [52.135]. The evanescent field will be completely attenuated at a particular angle of incidence corresponding to resonance and there will be no reflection. Figure 52.11 shows the SPR results when a spun film of nickel(II) tetrakis(4-cumylphenoxy)phthalocyanine (NiPc) molecules was subjected to a sequence of exposure to ozone (O_3) at 2 ppm. A period of 20 mins was allowed for the film to recover to its original state. The shift of the resonance angle $\Delta\theta_a$ was believed to be caused by a change in the refractive index of the film due to the interaction of O_3. $\Delta\theta_a$ is usually written in the form [52.136]

$$\Delta\theta_a = \frac{(2\pi/\lambda)(|\varepsilon_m|\varepsilon_i)^{3/2}d}{n_p \cos\theta(|\varepsilon_m| - \varepsilon_i)^2\varepsilon}(\varepsilon - \varepsilon_i)\,, \qquad (52.2)$$

where $|\varepsilon_m|$ is the modulus of the real part of the dielectric constant of the gold film; ε_i is the dielectric constant of the medium (air in this case) in contact with the organic thin layer of thickness d and the di-

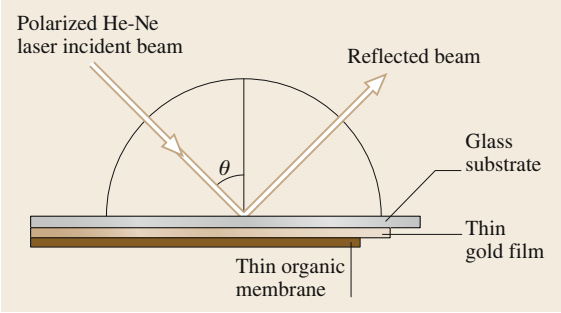

Fig. 52.10 A Kretschmann-type configuration for optical sensing interrogation

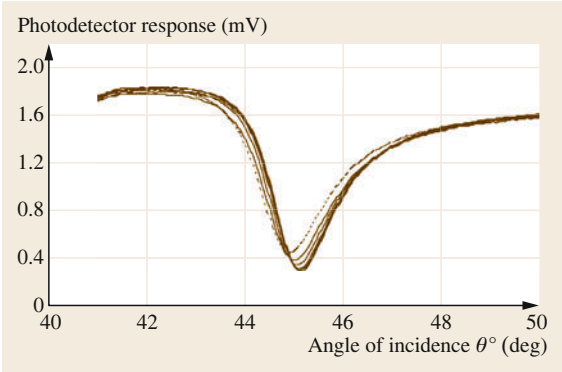

Fig. 52.11 The effect of a sequence of exposure at 20 min intervals of 2 ppm O_3 on a NiPc spun film. The *broken line* represents the system prior to exposure

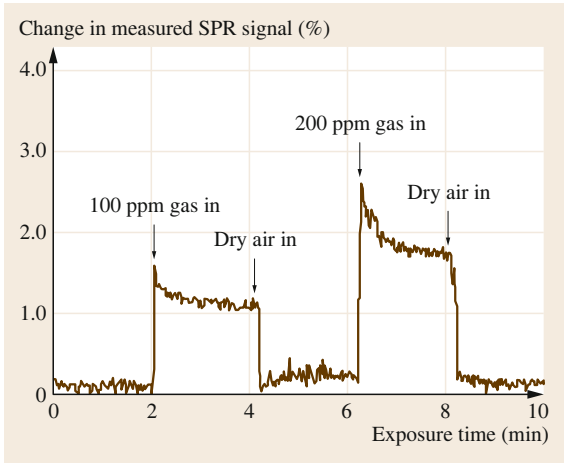

Fig. 52.12 Kinetics of the SPR response of copper hexadecafluorophthalocyanine ($CuPcF_{16}$) film to NH_3 gas at 100 ppm and 200 ppm. Measurements were at a fixed angle of $\theta^* = 46°$

electric constant ε. The resonance minimum moved to an increasingly larger angle after each exposure to ozone. The half-width became narrower at the same time and this was believed to be the consequence of oxidation of the phthalocyanine ring by ozone, which resulted in bleaching of the dye. SPR responses are in general slower and less readily reversible than semiconductivity changes but the technique is capable of providing additional information on the interaction between the gas and films as the shifts in both the angle and depth of the resonance can be monitored. Experimental data from the SPR response of CuPc films to nitrogen dioxide were input to a design process using an evolutionary algorithm. Gold layers with a thickness of 25 nm were found to exhibit 42.9% greater contrast than layers with a thickness of 50 nm. Using evolutionary design predictions, further modifications could be tested for available materials, and redundant layers may be eliminated. By inclusion of the external optics, a design could be selected to accommodate poor precision ($+/-0.5°$) in the incident angle and a possible multilayer solution was shown using Teflon AF 1600, with a refractive index similar to 1.3. The predicted NO_2 response showed an improvement compared with the classical SPR configuration, and the incident angle chosen by the genetic algorithm for the interrogation of these layers was close to a stationary point in the absolute response curve [52.137].

Figure 52.12 shows the transient response when thick films of copper hexadecafluorophthalocyanine ($CuPcF_{16}$) were exposed to 100 ppm of NH_3 for 2 min followed by the injection of dry air for a further 2 min period. The film was exposed to 200 ppm of NH_3 for the next cycle. The SPR response was very rapid and the recovery was complete. Unsubstituted CuPc was practically insensitive to this gas. Strong electron-withdrawing fluorine substituents made this substituted compound sensitive to reducing gases such as NH_3 [52.138].

SPR experiments were performed on films of different phthalocyanine derivatives in order to investigate the interaction mechanism with NO_2. SPR signal concentration as low as 1 ppm was measured using spun films of crown-ether-substituted phthalocyanines and octa-3,7,11-trimethyldodecyloxy phthalocyanine [52.139]. Adsorption of NO_2 took place both on the surface of the film and into the bulk. The surface adsorption increased the film thickness while the change in the real part of the film refractive index occurred due to the diffusion of NO_2 into the LB film. These processes were reversible and had no effect on the optical absorbance of the LB film. The SPR response of the bare Ag film to the exposure of NO_x (the equilibrium mixture of nitrogen dioxide and dinitrogen tetroxide) was slightly slower than the LB films of the tetra-4-*tert*-butyl-phthalocyanitosilicon dichloride (ttb-$PcSiCl_2$/Ag) system. This effect was associated with the high affinity of the phthalocyanine to NO_x gas. The NO_2 gas was also able to reach the Ag/Pc interface film and the reaction with the metal film resulted in the growth of a surface layer. This irreversible effect was found to be predominant during the recovery cycle and considerably reduced by the presence of a buffer LB layer of ω-tricosenoic (ω-TA) acid [52.140]. SPR studies showed that exposure of thin films of 18-crown-6 metal-free phthalocyanine molecules to NO_2 decreased the film absorbance. The optical permittivity of the NO_2-treated Pc over-layer was regarded as being an average of the optical permittivities of both components since the optical fields associated with surface plasmon po-

laritons sampled both the Pc and the NO_2 molecules. The disruption in the charge conjugation of the phthalocyanine molecules was observed because of the generation of organic radical cations as end products of the charge transfer during the physisorption process [52.141].

Using the excitation at wavelengths of 488 and 632.8 nm, SPR measurements were made on LB films of porphyrin molecules of EHO type deposited on an Ag-coated glass substrate. The resonance shift observed was larger at 488 nm than at 632.8 nm when the EHO films were exposed to NO_2 gas. The thickness and the complex dielectric constants at 632.8 nm were attributed to the island structure of the EHO LB films but the derived properties at 488 nm were believed to be caused by dispersion due to optical absorption [52.142]. Similar results were further obtained from UV-Vis absorption in these films [52.56].

52.4.3 Detection of Volatile Organic Vapor Compounds

Phthalocyanine molecules have also been extensively investigated for the recognition of volatile organic compounds (VOC). Langmuir–Blodgett (LB) and evaporated films of lutetium bisphthalocyanine ($LuPc_2$) molecules were deposited on indium tin-oxide (ITO) interdigitated electrodes in order to study the changes in their conductivity at room temperature due to the presence of a variety of organic vapors with different chemical functionalities. The results demonstrated the viability of the phthalocyanine thin films as the active species for systems specifically designed for the monitoring of aromatic components in food. The majority of the work on vapor sensing has, however, been based upon quartz crystal microbalance (QCM) transduction techniques. The frequency shift Δf from the nominal resonance frequency f_0 of the crystal due to the change in the mass Δm due to the adsorption of the vapors is [52.143]

$$\Delta m(\mathrm{mg/cm^2}) = \frac{\Delta f(\mathrm{Hz})}{2.26\times10^{-6} f_0^2} \,. \qquad (52.3)$$

It was demonstrated that monomeric soluble transition-metal phthalocyanines R_4PcM ($R =$ *tert*-butyl or 2,2-dimethyl-3-phenyl-propoxy) used as sensitive coatings for quartz microbalance transducers show reversible interaction and high sensitivity for organic solvents with high boiling point [52.144]. Quartz microbalance devices coated with LB films of copper(II) tetra-(*tert*-butyl)-5,10,15,20-tetraazaporphyrin exhibit good sensing response to the vapor of benzene and toluene at room temperature [52.145]. Soluble tetrakis-hexyl- and dodecylthiophthalocyaninato nickel(II) and the corresponding Pd(II) and Ag(I) complexes were investigated as sensitive materials for the detection of organic solvent vapors using quartz microbalance and interdigitated capacitance transducers. Sensor responses were found to be reversible at room temperature with response times on the order of several seconds depending on the partition coefficients of the organic solvents in the phthalocyanine film [52.146]. LB films of lanthanide diphthalocyanines such as praseodymium, ytterbium as well as octa-*tert*-butyl praseodymium diphthalocyanines were known to display spectroscopic changes when exposed to tobacco smoke [52.147]. The sensitivity and partition coefficient for ethanol, dichloromethane, acetone, and *n*-hexane were found to be larger for the QCM sensor using thermally annealed ordered membranes of octa(13,17-dioxanonacosane-15-sulfanyl)-substituted mesomorphic nickel(II) phthalocyanine molecules than as-coated untreated films. It was found from Raman spectroscopy that molecules with saturated C–C bonds such as ethanol interact with phthalocyanine films predominantly by the formation of hydrogen bonds and the sensor response to π-bond-containing compounds such as acetone is the result of their π–π interaction with the conjugated phthalocyanine ring [52.148].

Changes in refractive index of lutetium bisphthalocyanine ($LuPc_2$) in the presence of ethanol, hexanal, *n*-butyl acetate, and acetic acid were successfully exploited to produce an optical-fiber sensor operating at the wavelength of 1310 nm, capable of monitoring changes up to 10 dB in the reflected optical power for the detection of an 88 mmol/l concentration of acetic acid [52.149]. UV-Vis spectra of spin-coated layers of 29H,31H-(2,4-di-*t*-amylphenoxy)phthalocyanine, Zn(II) tetra-4-(2,4-di-*t*-amylphenoxy)phthalocyanine, and Zn(II) tris-(2,4-di-*t*-amylphenoxy)-[4-(4-mercapto-phenylimino-methyl)-phenoxy] phthalocyanine were found to be sensitive to *tert*-butylamine, diethylamine, dibutylamine, 2-butanone, and acetic acid. The selectivity was determined by both the metal and the peripheral substituents [52.150]. The synthesis of specially designed bispthalocyanine derivatives for VOC detection has been reported and their UV spectra are selectively sensitive to vapors depending on both the metal and the peripheral substituents. This observation has led to the fabrication of an *electronic optical nose* using an array of as-manufactured sensors for the analysis of some volatile organic compounds (VOC) that are of interest in food analysis [52.151].

The electrical conductivity of sol–gel-derived spun hybrid cobalt porphyrin-SnO_2 thin films showed a fast and reversible response to methanol vapors; the highest responses were observed at 250 °C. The porphyrin

was thermally stable up to 300 °C within the SnO_2 matrix and enhanced the methanol detection sensitivity at lower working temperatures. The incorporation of porphyrin into SnO_2 film had no effect on the detection of CO [52.152]. Hybrid thin films were produced using porphyrin and phthalocyanine and the response of absorption bands of the blend systems to the presence of VOCs was different from that obtained with a single compound [52.153].

Toluene vapor sensing has been successfully demonstrated using LB films prepared from copper tetrakis-(3,3-dimethyl-l-butoxycarbonyl) phthalocyanine (CuPcBC), copper tetrakis-(3,3-dimethyl-1-neopentoxycarbonyl) phthalocyanine (CuPcNC), and nickel tetrakis-(3,3-dimethyl-1-butoxycarbonyl) phthalocyanine molecules. Exposure to toluene resulted in a partially reversible shift in the resonance depth and position of the SPR curves and toluene could be detected down to at least 50 ppm [52.154].

52.4.4 Phthalocyanine for Biosensing

Immobilization of proteins on different surfaces offers a range of applications in biomedical engineering and the development of biosensors. The quantity and mode of adsorption of proteins are important characteristics of biomedical materials used for artificial blood vessels, heart, kidneys, and other organs after their implantation in the human body. Different surface properties of materials like roughness, charge, coverage, hydrophilicity, hydrophobicity, steric hindrance as well as structure, sign and charge of proteins influence protein adsorptions on implanted materials. Serum albumin, the most abundant protein in serum, has several functions for example, regulation of colloidal osmotic pressure of blood, transportation of fatty acids etc. It is often used as a stabilizer of dilute enzyme solutions, protein standard, cell culture media additive, blocking agent of nonspecific protein binding in enzyme-linked immunosorbent assay (ELISA) and Western blot [52.155].

The binding between bovine serum albumin (BSA) and phthalocyanine derivatives has already been studied by the measurements of fluorescence emission [52.156]. The interaction BSA and octahexylthio-substituted Cu(II) phthalocyanine derivative ($(C_6S)_8PcCu$) molecules has recently been reported by us and it was found that the mechanism involved a range of noncovalent interactions including hydrogen bonding especially with the nitrogen in the phthalocyanine ring, ionic interactions between negatively charged residues and the core metal ion, as well as Van der Waal's interactions. Heat treatment produced changes in the orientation of phthalocyanine stacks, making a favorable contribution to the protein adsorption and surface coverage profile [52.157]. The kinetics were measured for adsorption of lysozyme, bovine serum albumin, immunogamma globulin (IgG) on $(C_6S)_8PcCu$ films using a quartz crystal microbalance with dissipation technique. Lysozyme was found to reach to saturation value faster than BSA and IgG. The adsorption of IgGs on the phthalocyanine surface was much slower than that of BSA [52.158].

Using a CCD camera, the surface plasmon resonance imaging (SPRI) method has been employed to investigate BSA protein adsorption on spin coated films of liquid crystalline copper octakishexylthio phthalocyanines ($(C_6S)_8PcM$). Figure 52.13b,c shows the variation of reflected light intensity of these films with wavelength. Phosphate-buffered saline (PBS) washing is found to increase the resonance intensity. As shown in 52.13a, the blue shift in the resonance wavelength from 635 to 628 nm occurred due to PBS washing. As

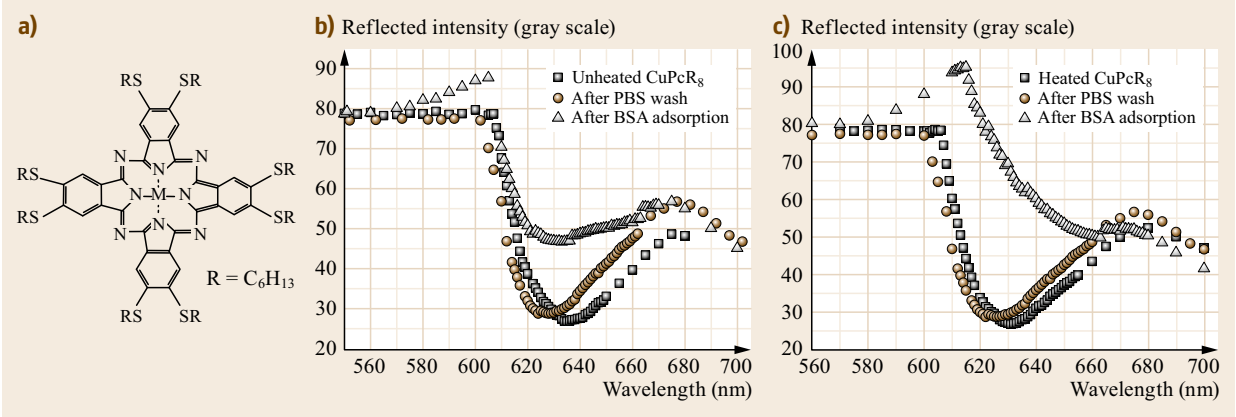

Fig. 52.13 (a) Molecular structure of octakisalkylthiophthalocyanine ($(C_6S)_8PcCu$). Reflected light intensity versus wavelength from SPRI measurements for BSA conjugation with $(C_6S)_8PcCu$ films as-deposited (b) and heated (c)

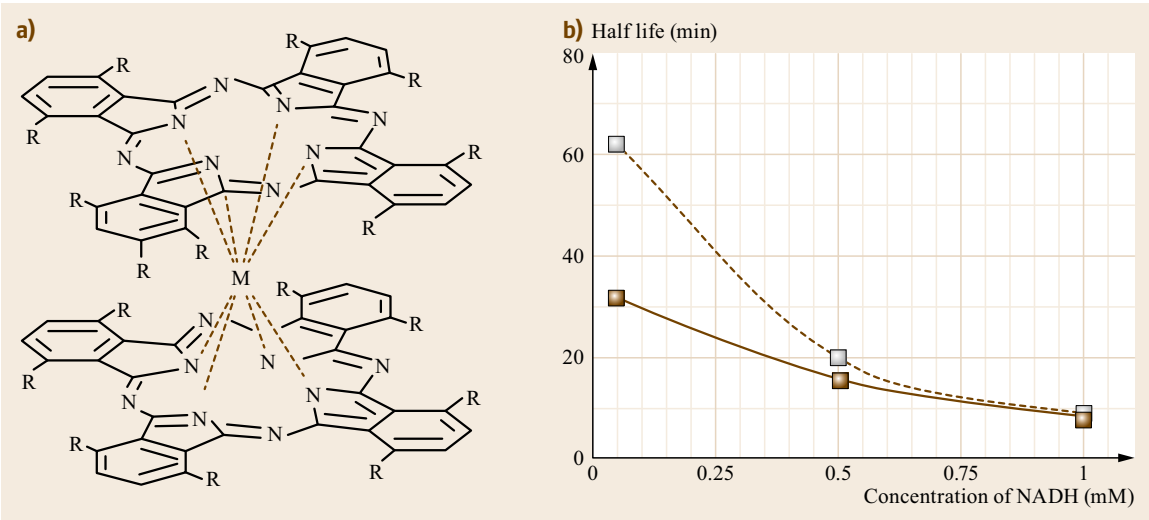

Fig. 52.14 **(a)** Chemical structure of C_8LuPc_2, M = Lu(III) and R = C_8H_{17}. **(b)** Dependence of oxidation half-life on NADH concentration for freshly prepared (*solid line*) and 3-month-old films (*dashed line*)

a result, salts of the PBS buffer are adsorbed on the film.

The reflected light color from the uneven film surface was visually yellowish green. The resonance was observed at 633 nm for the film after BSA adsorption. The mean intensity value for BSA adsorbed film increases up to 73% more than the phthalocyanine film. The spectrum was broader than that of the $(C_6S)_8PcCu$ overlayer because of the presence of damping. The shift in resonance wavelength from 622 to 663 nm was observed after BSA adsorption on the PBS-washed heated phthalocyanine film (Fig. 52.13c). The reflected color from the heat-treated film was visually more yellowish green than that from the as-deposited film. The surface coverage of the protein film and the amount of bounded BSA were higher than that obtained for the as-deposited $(C_6S)_8PcCu$ film. The calculated reflected intensity from the SPR image of the BSA film was increased by 170% at 631 nm compared to the phthalocyanine film. It is clear that the resonance curve is heavily damped for this film thickness. The BSA adsorbed onto the phthalocyanine film both before and after heat treatment was nonuniform as observed by SPRI as the substrate area was sufficiently large [52.159].

Spin-coated films, approximately 100 nm thick, of a newly synthesized bis[octakis(octyl)phthalocyaninato] lutetium(III) complex (chemical structure shown in Fig. 52.14) on ultrasonically cleaned glass substrates exhibit pronounced chemichromic behavior with potential application in health care. Oxidizing of a phthalocyanine film using Br_2 vapor or by applying a certain potential was shown to be effective by redshifts in optical absorption spectra. Using UV-Vis spectroscopy, a simple method was developed to detect NADH and vitamin C in a solution wetting the surface of an ITO-coated glass substrate modified with spin-coated electrochromic films [52.160]. The study showed satisfactory response times, and linear concentration ranges up to two orders of magnitude: 0.05−3 mM for NADH and 0.03−3.48 mM for vitamin C. The method of sensing NADH and vitamin C works well up to a concentration of 10^{-5} M and the complete recovery of the neutral bisphthalocyanine from the oxidized film via NADH reduction leads to the realization of developing reusable membranes. The reduction rate was greatly increased when redox biomolecules were added to the aqueous medium of water and $LiClO_4$. The reduction of the oxidized film in the presence of NADH and vitamin C was described in terms of first-order kinetics. The detection of NADH and vitamin C was found to be reproducible. As shown in Fig. 52.14b, the C_8LuPc_2 film remains sensitive for at least three months even when left in an open space.

52.5 Polymeric Materials

A polymer comprises of repeating molecules with the same chemical structure. The electrical conductivities of the intrinsically conducting polymer systems now range from 10^{-10}−10^{-5} S/cm. The common electronic feature of pristine conducting polymers is the π-conjugated system, formed by the overlap of carbon

p_z orbitals and alternating carbon–carbon bond lengths. Doping of the polymers can increase the conductivity to as high as 10^{+4} S/cm, a value comparable to that of a metal.

52.5.1 Conducting Polymers

Figure 52.15 shows the chemical structure of a few commonly used conducting polymers such as polyaniline, polypyrrole, and polythiophene for chemical sensors. In addition to the deposition techniques described earlier, conducting sensing filaments were produced using the scribbling and platinum-wire techniques [52.161]. Sensing membranes were also prepared by laser-induced chemical vapor polymerization [52.162].

LB films of stearic acid, a polyaniline oligomer (16-mer), and polypyrrole were deposited on the IDEs. Composite films of polyaniline and polypyrrole mixed with stearic acid in equal ratio by weight were also deposited on similar electrodes. Different brands of mineral water, tea, and coffee were sensed by impedance measurements on the films over the frequency range of

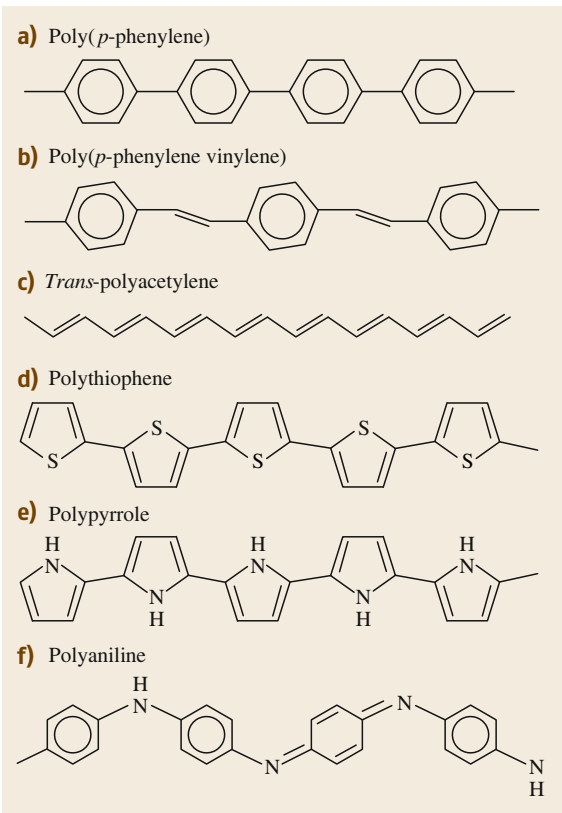

Fig. 52.15a–f Chemical structures of typical conducting polymers for sensors

20–10^5 Hz. The sensor arrays composed of these films were able to differentiate tastants below the human detection threshold [52.163]. The Brunauer, Emmett and Teller (BET) surface area for an amperometric polyaniline/Au/Nafion sensor prepared by the cyclic voltammetry (CV) method was found to be higher than structures prepared by the constant current (CC) method; the maximum sensitivity of CV-fabricated NO_2 gas sensors was 3.04 μA/ppm [52.164].

The type of doping is known to influence conducting-polymer-based sensors. Composite polyaniline emeraldine salts doped with an inorganic metal complex dopant, chromium(III) trioxalate (CTO) were produced by the chemical oxidative polymerization method. Polyanilines were also electrochemically doped with naphthalene-1,5-disulfonic acid (NSA). The conductivities of these materials were monitored by using the four-probe method when pellets of these materials were exposed to several saturated vapors of organic solvents for 30 min; the results are summarized in Fig. 52.16. The conductivity of the CTO-doped pellets was reduced by 18% on exposure to CH_2Cl_2 whereas the exposure had no effect on NSA-doped material. The response of undoped composite polyaniline salt to CH_2Cl_2 was also very small. Conversely, NSA-doped pellets showed a significant change in conductivity on exposure to CCl_4, while only very small changes were observed for the two other polymers. The responses to dimethylsulfoxide (DMSO) and *N*-methylpyrrolidone (NMP) were consistently higher for all three materials than the responses to the solvents

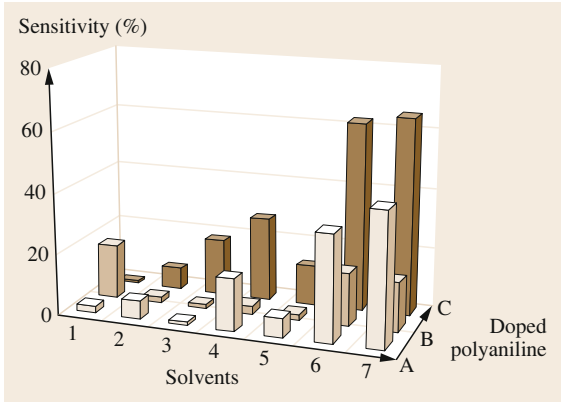

Fig. 52.16 Effects of vapor of: (1) dichloromethane (CH_2Cl_2), (2) chloroform ($CHCl_3$), (3) carbon tetrachloride (CCl_4), (4) acetonitrile (CH_3CN), (5) methanol (MeOH), (6) dimethylsulfoxide (DMSO), and (7) *N*-methylpyrrolidone (NMP) on the conductivity of: (A) pristine polyaniline emeraldine salt, and the salt doped with (B) chromium(III) trioxalate (CTO), and (C) naphthalene-1,5-disulfonic acid (NSA)

CH_3CN and methanol (MeOH). It became apparent that the interaction of solvents with the polyaniline salt became stronger with increasing polarity of the solvents. The response was reversible for all three materials. The nature of the dopant in the material and the consequent change in polarity, especially at the dopant site, and the resultant effect on π-electron delocalization and conductivity are primarily responsible for the characteristic sensing ability of the materials [52.165]. Extruded polymer blends containing polyaniline doped with dodecyl benzene sulfonic acid were dispersed in polystyrene (PSt) matrix filaments and the electrical conductivity of these filaments increased by a few orders of magnitude when exposed to a homologous series of alcohols, including methanol, ethanol, and 1-propanol. The effect was reproducible and recovery was satisfactory. The sorption of analyte molecules was believed to facilitate conduction through the insulating PSt moieties by enhancing charge-carrier mobility through hopping processes between adjacent polyaniline particles [52.166].

Multilayered thin films of polypyrrole were prepared by modifying a preformed Langmuir–Blodgett (LB) film of stearic acid by exposure to gaseous reactants such as hydrochloric acid and pyrrole vapors. A change in the electrical resistance of the film was observed when the film was exposed to polar molecules such as methanol, ethanol, and acetone, while the effect of nonpolar molecules on the resistivity of the film was found to be smaller. The response of LB films to exposure to ethanol was faster than that of electrochemically deposited polypyrrole, possibly due to the high ratio of surface area-to-bulk volume in the LB film [52.167]. Changes in mass and conductivity of polypyrrole thin films were measured to sense the primary alcohols [52.168].

Attempts have been made to integrate polyaniline optical sensor elements with optical communication technology for remote sensing by using 1300 nm as the operating wavelength. A 1% increase in transmission was observed at 1300 nm for electrochemically prepared polyaniline films when exposed to gaseous ammonia levels as low as 6 ppm at 50% relative humidity (RH). Different concentrations of ammonia were read by calibrating the sensors at intervals of 15 s. The response time was found to be insensitive to relative humidity variations in the range 30–70% [52.169]. Certain specially prepared polyaniline films showed partially reversible absorbance changes in the wavelength range 620–728 nm when exposed to 50–100 ppm of ozone at room temperature. The maximum sensitivity was attained at 620 nm. The cost-effective commercial exploitation of this effect was possible since the wavelength range was compatible with implementation on low-cost plastic optical fibers and small light sources [52.170].

Efforts have been invested in the use of information technology techniques to produce smart sensors. The sensor system, consisting of an acoustic two-port resonator operating at 433.92 and 380.8 MHz was configured as a frequency oscillator, including an integrated electronic module. The polymeric membranes were tested at room temperature for response to NO_2, NO, NH_3, CO, CH_4, SO_2, and H_2S in N_2. Responses to relative humidity (RH), and organic vapors (ethanol, acetone, and ethyl acetate) were also monitored. The sensitivity was found to be high. Principal component analysis (PCA) was performed to distinguish between different vapors of low concentrations [52.171]. Fluorescence emission from polymer-immobilized dye molecules on the multifiber tips was studied on exposure to organic vapors. Temporal responses were found to depend upon chemical nature (for example, polarity, shape, and size) of both the vapor and the polymer; these were used as input signals to train a neural network for vapor recognition. The system was able to identify individual vapors at different concentrations accurately [52.172]. Similar work was reported using the solvatochromic dye, Nile red. The dye was immobilized within various polymers. The substrate played a role in determining the sensitivity of the sensor. The sensitivity attained with microstructure glass (MSG) substrates was seven times greater than that with SU-8 photoresist-coated glass substrate and a 50% faster recovery was also achieved with the MSG substrates. The MSG sensor array was able to fingerprint the response for separate analytes with a high degree of repeatability. Using pattern-recognition techniques, sensor arrays were adaptable for gas identification and discrimination [52.173].

52.5.2 Ion Sensing

Water purification requires calibration of metal-ion contents. Polymeric ion-selective electrodes (ISEs) for Pb^{2+} incorporating *N*,*N*′-bis(salicylidene)-2,6-pyridinediamine with 2-nitrophenyl octyl ether and 50 mol% lipophilic additive were reported to have rapid response and excellent selectivity towards lead ions over other interfering metal ions [52.174]. *N*,*N*′-bis(5-methyl salicylidene)-*p*-diphenylene methane diamine formed a complex with Pb^{2+} and its selectivity was high, possibly due to the fact that the distance between the two nitrogen atoms and the position of the two hydroxyl groups is matched with the size of Pb^{2+} ions. ISEs based upon a dispersion of this Schiff base compound into the polyvinylchloride (PVC) membrane were characterized by a fast response time, a wide

linear dynamic range, and a fair selectivity coefficient with a slope of 29.4 mV per decade. The sensor had a low detection limit and an active life of three months without displaying considerable divergence in potentials [52.175]. A cleaned gold microelectrode was soaked in the freshly prepared solution of *o*-amino thiophenol (*o*-AT) and the metal nitrate of Cu, Hg, and Pb in *N*,*N*-dimethylformamide (DMF) for 4 h at room temperature. Simultaneous interaction took place between the thiophenol group of *o*-AT and the gold surface and its thiophenol and amino groups and M^{2+}. The ratio of 4 : 1 was found to be appropriate for *o*-AT:M^{2+} for the self-assembly of the *o*-AT on the gold surface and the formation of recognition cavities. The prepared ISEs showed specific selectivity to the template metal ions in mixed solutions containing the three heavy-metal ions. The limits of detection for ISEs were found to be 1.46×10^{-8} M, 3.73×10^{-8} M, and 4.34×10^{-8} M for Hg^{2+}, Cu^{2+} and Pb^{2+} ions, respectively [52.176]. Membranes containing five-layer LB films of tetracarboxylic perylene derivative and polypyrrole molecules were able to detect trace levels of Cu^{2+} ions in water [52.177]. The thiol-Cu-SAM particles were doped by the adsorption of thioxylenol or decanethiol into the porous polypyrrole film surface, resulting in an improvement in the sensitivity of the film to NH_3 [52.178]. Water-soluble regioregular polythiophenes containing acid C side chains were found to be suitable for the development of new Zn^{2+}, Mn^{2+}, and Cd^{2+} sensors [52.179].

52.5.3 Examples of Other Polymeric Sensors

A coordination polymer poly(CuMBSH) was formed via reaction of the bifunctional amphiphilic ligand, 5,5′-methylenebis (*N*-hexadecylsalicylideneamine) and copper ions at the water subphase. The response of LB films of poly(CuMBSH) to exposure of benzene, toluene, ethanol, and water was monitored by SPR measurements. The film became swollen, possibly due to the diffusion of solvent vapor into the polymer film. Poly(CuMBSH) is regarded as a relatively nonpolar material and its interactions were expected to be greater with vapors having a smaller dipole moment; the sensitivity increased with smaller dipole moment and higher refractive index of the vapor. The refractive index of the film increased because of an increase in the film density with the vapor filling the free volume inside the film. Similar results were obtained from admittance spectroscopic measurements on the same organic systems [52.180, 181].

The electrical properties of poly(methyl methacrylate) polymer (PMMA) films have been exploited for sensing applications (Fig. 52.17a shows the chemical formula). An increase in resistance of up to three orders of magnitude was observed for composite thin films of PMMA with carbon nanotubes when exposed to dichloromethane, chloroform, and acetone. The sensing mechanism is explained on the basis of volume expansion and polar interaction of various vapors on the nanotube surface [52.182, 183]. SPR measurements were made to investigate the room-temperature response of spun PMMA films to benzene, toluene, ethyl benzene, and *m*-xylene (BTEX) vapors under dynamic conditions. The response of PMMA to benzene was fast and reversible. The dissolution of benzene in the bulk of the polymer film formed a heterogeneous layer, primarily giving rise to swelling of the film and the value of the partition coefficient was estimated to be 112. Figure 52.18 shows that the increase in angular shift per ppm was linear with decreasing dipole moment of the solvent vapors. Benzene is a nonpolar solvent and toluene, ethyl benzene, and *m*-xylene are expected to show stronger solvation than benzene. Dissociated solvent ions may have formed a shell of bound ions and, as a result, the effective radius for dissolution in the polymer matrix would have increased. This dissociation might not easily occur for benzene, producing

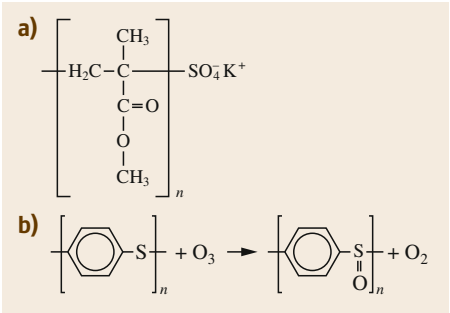

Fig. 52.17a,b Chemical structures of **(a)** poly(methyl methacrylate) derivatives and **(b)** reaction of polyphenylsulfide molecules with ozone

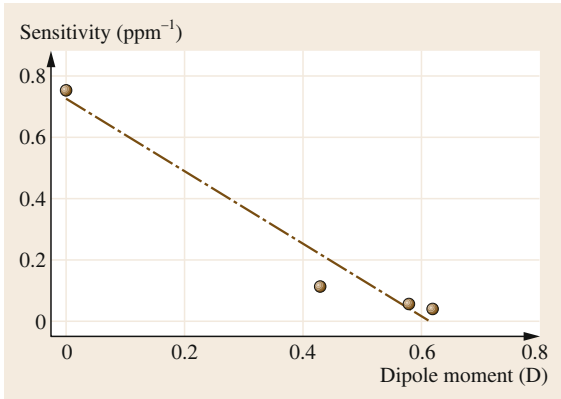

Fig. 52.18 Response of spun PMMA films on exposure to benzene (0 D), toluene (0.43 D), ethyl benzene (0.58 D), and *m*-xylene (0.62 D)

the highest SPR response [52.184]. A sensor has been made from a permselective poly(dimethylsiloxane) (PDMS) hollow-fiber membrane, showing a fast response time, very high oxygen permeability, and optimized oxygen/nitrogen selectivity. This sensor was suitable for monitoring the oxygen content in the outlet stream generated by medical oxygen concentration units [52.185].

Single-polyaniline films generally suffer from poor mechanical stability and polyaniline-blend films were prepared for practical applications using PMMA and PSt. The presence of water vapor, functioning as the interference gas, led to the lowering of the NH_3 response of the sensor in a humid atmosphere. The humidity effect was larger for PMMA than the PSt blend film. The difference was, however, not as large as expected from the water-sorption ability of PMMA [52.186]. The detection limits of ISE membranes with solid contacts are generally lower than a traditional liquid inner contact because of the diminished ion fluxes. Poly(methyl methacrylate)/poly(decyl methacrylate) (PMMA/PDMA) copolymer was employed as a solvent-cast membrane matrix on a layer of poly(*n*-octyl)thiophene (POT) deposited on Au as the internal contact. Ca^{2+}- and Pb^{2+}-selective electrodes were not sensitive to O_2 and the presence of a water film between the membrane and the internal contact was not found. The limits of detection were better by an order of magnitude and the response at low concentrations was much faster than for the liquid-contact electrode. For example, the drift was found to be smaller than 0.4 mV/min after 2 min when the concentration was increased from 10^{-9} to $10^{-7.7}$ M [52.187].

An amperometric hydrogen sensor was proposed using a proton-conducting solid polymer electrolyte membrane (PEM), a blend of palladium and platinum as the anode, and platinum as the cathode. The sensor operated as a fuel cell (H_2/Pd-Pt//PEM//Pt/O_2) and the short-circuit current was found to be linearly related to the hydrogen concentration [52.188].

It has recently been reported that thin films of polyphenylsulfide (PPS) (commercially termed noXon) act as efficient scrubbers of ozone from atmospheric ambient through the oxidation of the PPS molecules [52.189]. Thin films of this compound are found to be a useful material for the fabrication of sensing membranes suitable for the detection of ground-level ozone at concentrations of a few ppm or even lower [52.190, 191]. A 1 h exposure to 2 ppm of O_3 was shown to cause at least a 1.1% change in the refractive index of the film [52.192]. As shown in Fig. 52.17b, oxidation of the PPS polymer by ozone exposure results in an irreversible increase in the index of refraction of the polymer [52.193].

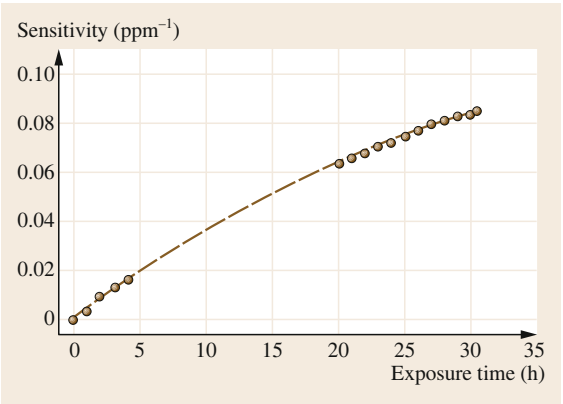

Fig. 52.19 Time-dependence behavior of ozone sensitivity of PPS films. Two sets of hourly readings, separated by 16 h of continuous exposure without SPR measurements (*dashed line*)

Figure 52.19 shows the results of SPR measurements on PPS films when exposed to 1.5 ppm ozone. The increase in the refractive index Δn was found to be linear over the first few hours of exposure with an estimated slope of 10^{-4} refractive index units (RIU)/min. The sensitivity was defined as the ratio of Δn to the concentration of ozone. The interaction of O_3 with PPS films is believed to be an accumulative effect and such mechanisms can therefore serve as both a scavenger as well as an indicator of ozone in a certain ambient. The density of the binding of oxygen to a PPS film after 5 h of exposure to 2 ppm ozone was estimated from QCM measurements to be about 5×10^{18} cm^{-3}.

Electrospun nanofibers with diameters of 100–400 nm were deposited on the surface of a QCM by electrospinning homogenous blend solutions of crosslinkable poly(acrylic acid) (PAA) and poly(vinyl alcohol) (PVA). The NH_3 sensing properties were mainly affected by the content of the PAA component in the nanofibrous membranes, the concentration of NH_3, and relative humidity. The sensitivity of nanofibrous-membrane-coated QCM sensors was also much higher than that of continuous-film-coated QCM sensors [52.194].

Molecularly imprinted polymers (MIPs) are now well recognized as robust, cost-effective, and highly durable synthetic receptors for specific targets having variable sizes and shapes. MIPs which provide interaction points and a coordination sphere around the template molecule have applications ranging from liquid chromatography to assay and sensor technologies and drug delivery [52.195].

The synthesis method of MIPs includes the selection of the required target molecule used as the molecular template, and embedded in the presence of

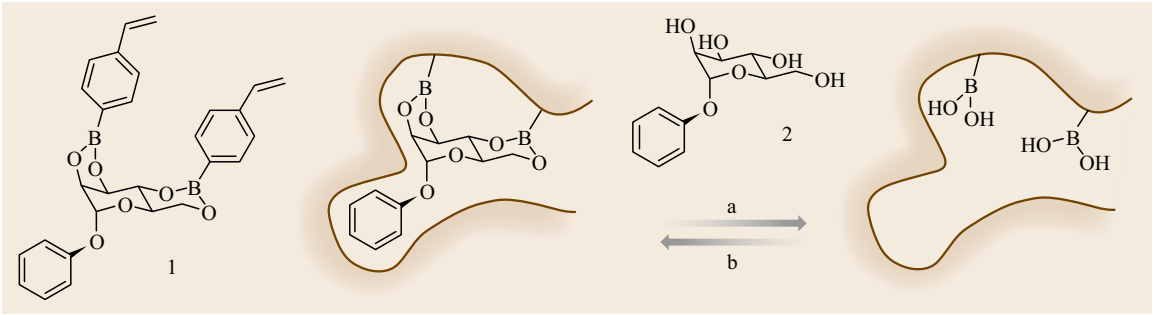

Fig. 52.20 Schematic representation of a cavity obtained by polymerization (1) starting molecule (2) formation of cavity (a) and (b) route to successive chemical formation

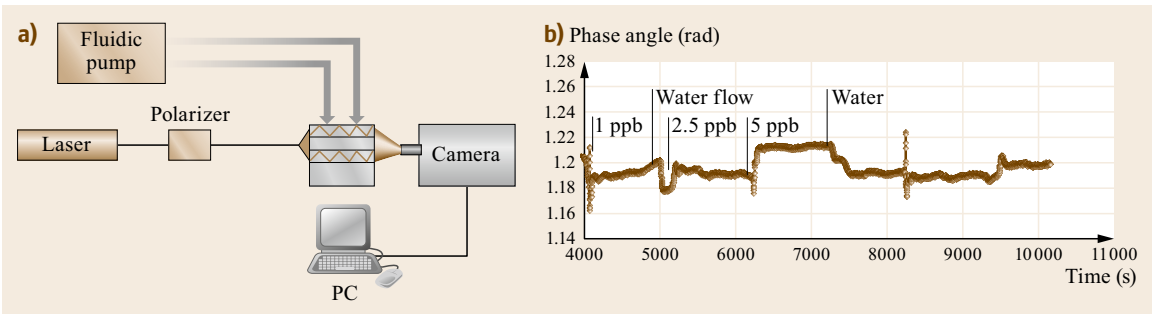

Fig. 52.21 **(a)** Schematic diagram of dual polarization interferometer (DPI) **(b)** DPI time trace transverse electric phase angle in radians upon adding 1, 2.5 and 5 ppb atrazine to atrazine MIP immobilized on a DPI chip

functional monomers, whereby the monomers interact with and engross into sites of the template forming a complex followed by further polymerization. After the completion of the polymerization the functional sites of the molecule template are held in position and surrounded by the highly crosslinked polymeric structure, followed by the removal process of the template molecule which subsequently results in the formation of cavities, specific in size, shape, and chemical functionality of the target molecule (Fig. 52.20). These imprinted functional cavities are then capable of identifying, rebinding, and quantifying the target molecules with excellent degrees of selectivity and sensitivity and are therefore an ideal immobilization method of sensor layers [52.196].

For the specific detection and quantification of the herbicide atrazine, a triazine molecule is used as the template molecule and reacted with the monomer methacrylic acid (MAA) in addition to the crosslink agent ethylene glycol dimethacrylate (EGDMA) initiated by azobisisobytyronitrile (AIBN) during the synthesis process. The polymerization is driven and influenced by heat, whereby the triazine molecule is removed by Sox extraction using acetic acid and chloroform. The optimization process of the final MIP influences the guest capacity factor, as some of the functional sites present remain inaccessible due to the presence of residual template molecules, excessive crosslinking restricting the diffusion or deformation of the network during the extraction process by swelling or relaxation caused by the solvent. Under these influences the guest capacity for MIPs is limited with typical values of 0.1 mg per 1 mg of MIP, however advanced polymeric systems with trifunctional crosslinker agents or higher offer significant increases in capacity which in turn enhances the recognition and decreases possible retention times. The selection of the optimal solvent also plays an essential role in the type of interaction involved and consequently determines its polarity and dissociating energy, capable of influencing the morphology of the material during synthesis, including the size, shape, and quantitative distribution of the cavities. It is therefore crucial during analysis stages to incorporate a solvent similar to the synthesis solvent involved in the production of the original network in order to exclude the possibility of restructuring the effective morphology and to obtain the selectivity to the initial degree [52.197].

Atrazine is a man-made chemical which is very widely used as a herbicide. It can be harmful to wildlife, is long-lasting in the environment, and a potential groundwater contaminant. Commercially available

molecularly imprinted polymer (MIP) is dispersed into the chloroform solution of poly(methyl methacrylate) (PMMA) to produce the sensing membrane for the herbicide atrazine. The interaction of MIP/PMMA matrices with atrazine was investigated using the dual polarization interferometric (DPI) technique (as shown schematically in Fig. 52.21a). The interferometer is able to interrogate the sensor/sample interface by coupling transverse electric (TE) and transverse magnetic (TM) waves representing light parallel and perpendicular to the plane of the chip [52.198]. A thin film of MIP dispersed in PMMA solution was spin-coated onto the silicon oxynitride surface of the DPI chip. Distilled water was used as the running buffer and this was switched to 400 µl injections of 1 ppb of atrazine in solution. The running buffer was switched back to distilled water following completion of each injection loop. As shown in Fig. 52.21b), it was possible to measure the change in phase due to increasing exposure levels of atrazine. The atrazine effect was effectively removed by switching the running buffer back to distilled water. This suggested that the detection of atrazine by the MIP/PMMA thin film integrated to the DPI chip was reversible. However, given that the bound atrazine could be removed by a simple water wash suggests that the herbicide was not strongly bound to the MIP trapped in the PMMA film. Normally a more stringent elution stage is required to remove the atrazine from the MIP.

52.6 Cavitand Molecules

Thin films of some novel cavitand compounds such as crown ethers [52.199] and calixarenes [52.200, 201] can form inclusion complexes with some organic guest molecules. This effect is being extensively exploited for the development of sensors for organic vapors [52.202, 203]. Thin films can be prepared using LB film deposition, spin coating, and self-assembly techniques [52.204–207]. The nanoporous flexible structure of thin LB films of amphiphilic calixresorcinarene derivatives were found to provide a suitable matrix for the incorporation of aromatic molecules [52.208]. This adsorption process was very fast, and full recovery of the film was observed after flushing with clean air. It has to be pointed out, however, that the detected vapors were of a high concentration (a few percent by volume) and the adsorption was not selective since all vapors studied yielded a similar response. However, this may lead to the development of a sensor for explosives, where specificity is not considered relevant. These effects are attributed to weak and nonspecific interactions between the guest molecules and the calixarene LB film. It was also shown that the adsorption of organic vapors occurs in the whole bulk of the LB films, and that the number of adsorbed molecules is much higher than the number of calixarene molecules [52.209]. The adsorption mechanism involved the swelling of the film and even condensation of the adsorbate within the film. The swelling of the film was confirmed by independent measurements using ellipsometric and surface plasmon resonance (SPR) techniques [52.210]; the adsorption mechanism still remained unclear. For all the studied analytes, the number of adsorbed molecules was found to be much larger than that expected from the geometrical dimensions of the intrinsic calixarene cavity and the empty space between the molecules. This discrepancy was explained by either film swelling or the condensation of vapor molecules inside the film, or both [52.208]. Spun films of calixresorcinarenes, however, were found to be homogeneous, and the porosity of the film was similar to that of LB-deposited films. Both LB and spun films of comparable thickness exhibited similar SPR response on exposure to toluene vapor [52.62]. Prolonged irradiation of the CA films with a focused laser beam caused an initial increase in film sensitivity to various organic vapors [52.211].

Figure 52.22 shows the chemical structure of an amphiphilic calixresorcinarene derivative with several different types of substituents. Exposures of layers of CAs to vapors of benzene, ethylbenzene, toluene, and *m*-xylene in low concentrations produced changes in the optical properties, i. e., the film thickness and refractive index of the layers. Fast response and recovery processes have been observed, with response times as short as a few seconds. The normalized SPR responses are shown in the three-dimensional (3-D) diagram in Fig. 52.23. It is apparent that the interaction of the analyte was, in general terms, specific to the thin film of a particular CA derivative. The adsorption mechanism was interpreted in terms of the accumulation of the vapor molecules in the liquid phase inside the film matrix, probably caused by capillary condensation in the porous structure of the CA films [52.212]. These LB films had a characteristic pore size of about 1 nm. Condensation of vapor occurred inside capillaries similar to the porous structure of calixarene films at pressures lower than their saturated pressure at a certain temperature. The saturated vapor pressures of ethylbenzene and *m*-xylene are similar and therefore their exposure to the CA derivatives produced similar effects. Conversely, benzene, with the highest saturated

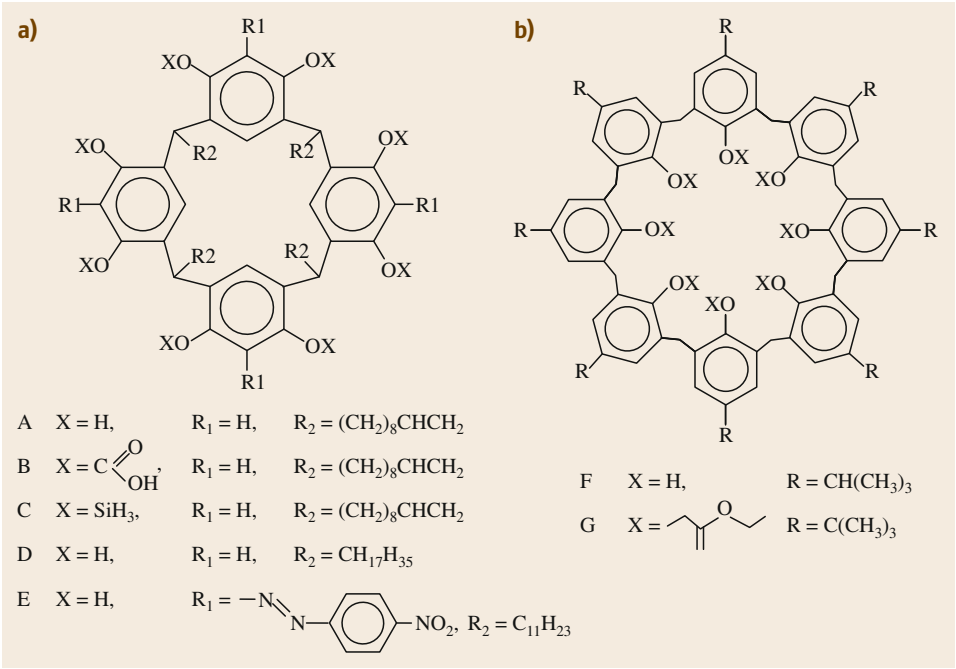

Fig. 52.22a,b Chemical formulae of calixresorcinarene derivatives

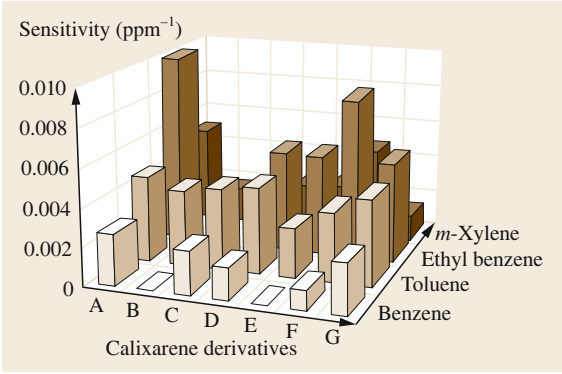

Fig. 52.23 A 3-D representation showing the response of different calixarene derivatives to different organic vapors (benzene (B), *m*-xylene (X), toluene (T), and ethylbenzene (E)) at a concentration of 375 ppm

vapor pressure, yielded the smallest detectable SPR signal.

Composite LB films of amphiphilic CA and PPS were exposed to 2 ppm of O_3 [52.190]. The competition between the permanent oxidation process of the PPS polymer by the adsorbed O_3 molecules and the release of O_3 from the CA matrix was found to depend on the molar ratios of the CA and PPS compounds. Recovery became slower with lower CA proportions in the film matrix.

The conductivity of the CA derivative is intrinsically low. CA films were deposited on the gate between the source and the drain of a charge-flow transistor and the turn-on response for the transistor upon exposure to organic solvent was recorded. The increase in the membrane conductivity is partially attributed to condensation of the vapors in the highly microporous membrane even below the saturation vapor pressure and partially to the effect of the polar analyte molecules complexing inside and between the OH groups of the cavities. The technique offers several advantages over existing methods:

1. Immunity to water vapor, because of the hydrophobic nature of the membrane
2. No catalytic poisoning of the membrane, as is commonly observed for doped SnO_2
3. No accumulative effects, which are responsible for baseline drift in quartz-crystal-type sensors, are observed
4. No porous metal layer, the adhesion of which may be prone to degradation, is needed on top of the membrane [52.213].

52.7 Concluding Remarks

The scope of organic materials for chemical sensing is huge and it is impossible to provide a complete description of these materials. Electronic artificial noses are being developed as systems for the automated detection and classification of odors, vapors, and gases. These instruments consist of three main components:

1. An array of chemical membranes
2. Electronic circuitry for data acquisition, signal processing, and display
3. A pattern-recognition algorithm.

Up-to-date information on applications of materials for electronic noses and tongues is available in a recent review [52.214]. Problems associated with human senses are many: individual variability, impossibility of online monitoring, subjectivity, adaptation, infections, harmful exposure to hazardous compounds, and mental state. These limitations can be overcome by developing intelligent sensor systems. Gas sensors tend to have very broad selectivity, responding to many different analytes of varied concentrations. The electronic nose/tongue, therefore, offers a definite advantage in many applications in the food and utility industries, the health care and medical care sectors, and security services. The demand for advanced electronic noses will continue to stimulate the search for novel sensing materials.

Mathematical and computational tools are expected increasingly to play a part in the design of advanced electronic-nose systems. An electronic nose has been developed to monitor breathing air in human habitats. A molecular modeling study was undertaken to investigate the interactions between resistive sensors of a polymer–carbon black (CB) composite and analytes. Poly(4-vinylphenol), polyethylene oxide, and ethyl cellulose were considered for modeling, based on their stereoisomerism and sequence isomerism. The CB was modeled as uncharged naphthalene rings with no hydrogen. Molecular mechanical and molecular dynamics techniques were employed and the equilibrium composite structure was constructed by inserting naphthalene rings into the polymer matrix. The radial distribution profiles produced information on the composite microstructure. The sensor response was predicted in terms of the interaction energies of the analytes with the composites. Studies included both inorganic and organic analytes [52.215].

Research efforts are also growing in the mineralization of VOC pollutants to innocuous compounds [52.216]. Visible-light-assisted removal of organic pollutants by photocatalytic action of dye-sensitized TiO_2 surfaces offers several attractive advantages. Firstly, the nanoscale device architecture is versatile with several methods of solar energy conversion whilst producing a chemical fuel in the form of pure H_2. Secondly, pollutant species and concentrations of mixtures in industrial waste streams can be identified [52.217]. Results so far reported are encouraging. For example, 40–75% degradation of aromatic pollutants such as phenol, chlorophenol, trichloroethylene, and surfactants was achieved with TiO_2 surfaces modified by methylene blue and rhodamine B dyes after less than 5 h of irradiation with a 150 W xenon lamp [52.218]. Individual VOCs including methylene chloride, ethanol, benzene, acetone, xylene, and isopropanol produced unique signatures as they were oxidized on the sensor surface [52.219]. Interest in hybrid hetero-supramolecular structures will therefore remain alive for the foreseeable future.

Acknowledgments. The author is grateful to the Engineering & Physical Research Council (UK) and the European Union for financial support of their work over the last 20 years. Gratitude is also due to Dr. S. C. Thrope of the Health Safety Executive (UK), Dr. M. Hofton of TQ Environmental Plc., Prof. K. C. Thompson of ALControl, and Dr. F. A. Grunfeld of NIMA Technology for their collaboration and support. Prof. M. J. Cook of the University of East Anglia has remained a generous provider of novel phthalocyanine compounds for sensing experiments over the years. The contributions from Drs. R. Capan, O. Omar, and A. V. Nabok are acknowledged with gratitude. Above all, the author is enormously indebted to his parents Chittarajan and Sarashi of Belgram (India) for stimulating his interest in academic career in science.

References

52.1 W. Gopel: Sensors Actuat. B **18/19**, 1 (1994)
52.2 M.C. Petty: Biosens. Bioelectron. **10**, 129 (1995)
52.3 M.J. Cook: Chem. Rec. **2**(4), 225 (2002)
52.4 L. Alcacer: *Conducting Polymers Special Applications* (Reidel, Dordrecht 1987)
52.5 E.B. Feresenbet, E. Dalcanale, C. Dulcey, D.K. Shenoy: Mol. Cryst. Liq. Cryst. **397**, 585 (2003)
52.6 N.K. Hunt, B.J. Marinas: Water Res. **31**, 1355 (1997)

52.7 T. Oshima, K. Sato, H. Terauchi, M. Sato: J. Electrostat. **42**, 159 (1997)
52.8 N. Carmona, M.A. Villegas, J.M.F. Navarro: Sensors Actuat. A Phys. **116**(3), 398 (2004)
52.9 N. Carmona, M.A. Villegas, J.M.F. Navarro: Thin Solid Films **458**(1/2), 121 (2004)
52.10 C.L. Baban, Y. Toyoda, M. Ogita: Jpn. J. Appl. Phys. **143**(10), 7213 (2004)
52.11 I. Toma-Dasu, U. Dasu, M. Karlsson: Phys. Med. Biol. **49**(19), 4463 (2004)
52.12 S.E.J. Williams, P. Wootton, H.S. Mason, J. Bould, D.E. Iles, D. Riccardi, C. Peers, P.J. Kemp: Science **306**(5704), 2093 (2004)
52.13 F. Bender, C. Kim, T. Mlsna, J.F. Vetelino: Sensors Actuat. B Chem. **77**(1/2), 281 (2001)
52.14 B. Onida, L. Borello, S. Fiorilli, B. Bonelli, C.O. Arean, E. Garrone: Chem. Commun. **21**, 2496 (2004)
52.15 S. Sen, K.P. Muthe, N. Joshi, S.C. Gadkari, S.K. Gupta, M. Jagannath: Roy, S. K. Deshpande, J. V. Yakhmi: Sensors Actuat. B, Chem **98**(2/3), 154 (2004)
52.16 B.H. Timmer, K.M. van Delft, R.P. Otjes, W. Olthuis, A. van den Berg: Anal. Chim. Acta **507**(1), 137 (2004)
52.17 M. Beekmann, G. Angellet, G. Megie, H.G.J. Smith, D. Kley: J. Atmos. Chem. **19**, 259 (1994)
52.18 L. Xie, T.J. Lu, H.Q. Yan: Electroanal. **10**, 842 (1998)
52.19 T. Becker, L. Tomasi, C. Bosch v. Braunmühl, G. Müller, G. Sberveglieri, G. Fagli, G. Fagli: L. Tomasi, C. Bosch v. Braunmühl, G. Müller, G. Sberveglieri, G. Fagli, E. Comini, Sensors Actuat. A Phys **74**, 229 (1999)
52.20 H. Schulz, G.B. De Melo, F. Ousmanov: Combust. Flame **118**, 179 (1999)
52.21 B. Zielinska, J.C. Sagebiel, G. Harshfield, A.W. Gertler, W.R. Pierson: Atmos. Environ. **30**, 2269 (1996)
52.22 F.B. Reig, J.V. Adelantado, V.P. Martinez, M.C. Moreno, M.T. Carbo: J. Molec. Struct. **480/481**, 529 (1999)
52.23 W. Groves, E.T. Zellers, G.C. Frye: Anal. Chim. Acta **371**, 131 (1998)
52.24 W.A. Groves, E.T. Zellers: Ann. Occup. Hyg. **45**, 609 (2001)
52.25 N. Kasai, I. Sugimoto, M. Nakamuro, T. Katoh: Biosens. Bioelectron. **14**, 533 (1999)
52.26 G. Sberveglieri: Sensors Actuat. B **23**, 103 (1995)
52.27 D. Manno, A. Serra, M. Di Giulio, G. Micocci, A. Tepore: Thin Solid Films **324**, 44 (1998)
52.28 N. Taguchi: Japanese Patent Application No. 45-38200 (1962)
52.29 C.D. Kohl, A. Eberheim, P. Schieberle: Tech. Mess. **71**(5), 298 (2004)
52.30 A. Eberheim, D. Kohl, P. Schieberle: Phys. Chem. Chem. Phys. **5**(23), 5203 (2003)
52.31 J. Gutierrez, J. Getino, M.C. Horrillo, L. Ares, J.I. Robla, C. Garcia, I. Sayago: Thin Solid Films **317**, 429 (1998)
52.32 M. Graf, D. Barrettino, S. Taschini, C. Hagleitner, A. Hierlemann, H. Baltes: Anal. Chem. **76**(15), 4437 (2004)
52.33 E. Comini, G. Faglia, G. Sberveglieri, Z. Pan, Z.L. Wang: Appl. Phys. Letts. **81**(10), 1869 (2002)
52.34 A. Gramm, A. Schutze: Sensors Actuat. B Chem. **95**(1-3), 58 (2003)
52.35 O.K. Varghese, D. Gong, M. Paulose, K.G. Ong, C.A. Grimes: Sensors Actuat. B Chem. **93**, 338 (2003)
52.36 A.K. Prasad, P.I. Gouma: J. Mater. Sci. **38**(21), 4347 (2003)
52.37 K.S. Novoselov, A.K. Geim, S.V. Morozov, D. Jiang, Y. Zhang, S.V. Dubonos, I.V. Grigorieva, A.A. Firsov: Science **306**(5696), 666 (2004)
52.38 J.F. Ping, Y.B. Zhou, Y.Y. Wu, V. Papper, S. Boujday, R.S. Marks, T.W.J. Steele: Biosens. Bioelectron. **64**, 373 (2015)
52.39 S.G. Chatterjee, S. Chatterjee, A.K. Ray, A.K. Chakraborty: Sens. Actuator B-Chem **221**, 1170 (2015)
52.40 Y.Y. Shao, J. Wang, H. Wu, J. Liu, I.A. Aksay, Y.H. Lin: Electroanalysis **22**(10), 1027 (2010)
52.41 M.J. Lu, J. Li, X.Y. Yang, C.A. Zhang, J. Yang, H. Hu, X.B. Wang: Chin. Sci. Bull. **58**(22), 2698 (2013)
52.42 J. Byun: J. Microbiol. Biotechnol. **25**(2), 145 (2015)
52.43 T. Kuila, S. Bose, P. Khanra, A.K. Mishra, N.H. Kim, J.H. Lee: Biosens. Bioelectron. **26**(12), 4637 (2011)
52.44 N.B. McKeown: *Phthalocyanine Materials. Synthesis, Structure and Function* (Cambridge Univ. Press, Cambridge 1998)
52.45 S. Tabuchi, H. Tabata, T. Kawai: Surf. Sci. **571**(1-3), 117 (2004)
52.46 M. Szybowicz, T. Runka, M. Drozdowski, W. Bala, A. Grodzicki, P. Piszczek, A. Bratkowski: J. Molec. Struct. **704**(1-3), 107 (2004)
52.47 A. Boguta, D. Wrobel, A. Bartczak, R. Swietlik, Z. Stachowiak, I.M. Ion: Mater. Sci. Eng. B Solid **113**(1), 99 (2004)
52.48 J. Spadavecchia, G. Ciccarella, S. Capone, R. Rella: Chem. Mater. **16**(11), 2083 (2004)
52.49 H. Nishimura, M. Iizuka, S. Kuniyoshi, M. Nakamura, K. Kudo, K. Tanaka: Electron. Commun. Jpn. **87**(2), 18 (2004)
52.50 Y.L. Lee, H.Y. Wu, C.H. Chang, Y.M. Yang: Thin Solid Films **423**(2), 169 (2003)
52.51 M.C. Petty: *Langmuir-Blodgett Films: An Introduction* (Cambridge Univ. Press, Cambridge 1996)
52.52 M.J. Cook: J. Mater. Sci. Electron. **5**, 117 (1994)
52.53 M.J. Cook: Int. J. Electron. **76**, 727 (1994)
52.54 C.G. Claessens, W.J. Blau, M. Cook, M. Hanack, R.J.M. Nolte, T. Torres, D. Wohrle: Monatsh. Chem. **132**(1), 3 (2001)
52.55 M.J. Cook: J. Mater. Chem. **6**, 677 (1996)
52.56 T.H. Richardson, C.M. Dooling, O. Worsfold, L.T. Jones, K. Kato, K. Shinbo, F. Kaneko, R. Tregonning, M.O. Vysotsky, C.A. Hunter: Colloid Surf. A **198**, 843 (2002)
52.57 M.J. Cook, J. McMurdo, D.A. Miles, R.H. Poynter, J.M. Simmons, S.D. Haslam, R.M. Richardson, K. Welford: J. Mater. Chem. **4**, 1205 (1994)
52.58 A.K. Hassan, A.K. Ray, A.V. Nabok, S. Panigrahi: IEE Proc.-Sci. Meas. Technol. **147**, 137 (2000)
52.59 D. Meyerhofer: J. Appl. Phys. **49**, 3993 (1978)
52.60 P.C. Sukanek: J. Elechtrochem. Soc **138**, 1712 (1991)

52.61 P.C. Sukanek: J. Electrochem. Soc. **144**, 3959 (1997)
52.62 A.K. Hassan, A.V. Nabok, A.K. Ray, A. Lucke, K. Smith, C.J.M. Stirling, F. Davis: Supramol. Sci. Mater. Sci. Eng. C **8/9**, 251 (1999)
52.63 S.M. Critchley, M.R. Willis, M.J. Cook, J. McMurdo, Y. Maruyama: J. Mater. Chem. **2**, 157 (1992)
52.64 G.C. Bryant, M.J. Cook, C. Ruggier, T.G. Ryan, A.J. Thorne, S.D. Haslam, R.M. Richardson: Thin Solid Films **243**, 316 (1994)
52.65 X. Li, H. Xu, Q. Zhou, D. Jiang, L. Zhang, A. Lu: Thin Solid Films **324**, 277 (1998)
52.66 K. Bandyopadhyay, S.G. Liu, H.Y. Liu, L. Echegoyen: Chem. Eur. J. **6**, 4385 (2000)
52.67 C.C. Hsueh, M.T. Lee, M.S. Freund, G.S. Ferguson: Angew. Chem. Int. Ed. **39**, 1228 (2000)
52.68 H.G. Hong, M. Jiang, S.G. Sligar, P.W. Bohn: Langmuir **10**, 153 (1994)
52.69 K.F. Kelly, Y.B.S. Shon, T.R. Lee, N.J. Halas: J. Phys. Chem. B **103**, 8639 (1999)
52.70 V. Poderys, A. Selskis, R. Rotomskis: Solid State Phenom. **97/98**, 221 (2004)
52.71 A. Ulman: *An Introduction to Ultrathin Films: From Langmuir–Blodgett to Self-Assembly* (Academic, SanDiego 1991)
52.72 T.R.E. Simpson, D.A. Russell, I. Chambrier, M.J. Cook, A.B. Horn, S.C. Thorpe: Sensors Actuat. B **29**, 353 (1995)
52.73 M.J. Cook: Pure Appl. Chem. **71**(11), 2145 (1999)
52.74 K. Ozoemena, P. Westbroek, T. Nyokong: J. Porphyr. Phthalocyan. **6**(2), 98 (2002)
52.75 X. Zhang, J.C. Shen: Adv. Mater. **11**(13), 1139 (1999)
52.76 Y. Lvov, G. Decher, H. Möhwald: Langmuir **9**, 481 (1993)
52.77 Y. Lvov, K. Ariga, I. Ichinose, T. Kunitake: J. Am. Chem. Soc. **117**, 6117 (1995)
52.78 Y.M. Lvov, G. Decher: Crystallogr. Rep. **39**, 628 (1994)
52.79 X. Zhang, M.L. Gao, X.X. Kong, Y.P. Sun, J.C. Shen: J. Chem. Soc. Chem. Commun. **9**, 1055 (1994)
52.80 C.Q. Sun, X.Y. Zhang, D. Jiang, Q.A. Gao, H.D. Xu, Y.P. Sun, X. Zhang, J.C. Shen: J. Electroanal. Chem. **411**(1/2), 73 (1996)
52.81 D.J. Revell, I. Chambrier, M.J. Cook, D.A. Russell: J. Mater. Chem. **10**(1), 31 (2000)
52.82 M.J. Cook, I. Chambrier: Phthalocyanine properties. In: *The Porphyrin Handbook*, Vol. 17, ed. by K.M. Kadish, K.M. Smith, R. Guilard (Academic, New York 2003) p. 38
52.83 S. Antohe, N. Tomozeiu, S. Gogonea: Phys. Stat. Sol. (a) **125**, 397 (1991)
52.84 M.J. Cook, M.F. Daniel, K.J. Harrison, N.B. Mckeown, A.J. Thomson: J. Chem. Soc. Chem. Commun. **15**, 1148 (1987)
52.85 M.J. Cook, M.F. Daniel, K.J. Harrison, N.B. Mckeown, A.J. Thomson: J. Chem. Soc. Chem. Commun. **14**, 1086 (1987)
52.86 A.K. Ray, A.V. Nabok, A.K. Hassan, O. Omar, R. Taylor, M.J. Cook: Philos. Mag. B **78**(1), 53 (1998)
52.87 X.B. Huang, Y.Q. Liu, S. Wang, S.Q. Zhou, D.B. Zhu: Chem. Eur. J. **8**(18), 4179 (2002)
52.88 C. Granito, L.M. Goldenberg, M.R. Bryce, A.P. Monkman, L. Troisi, L. Pasimeni, M.C. Petty: Langmuir **12**(2), 472 (1996)
52.89 B.N. Achar, P.K. Jayasree: Can. J. Chem./Rev. Can. Chim. **77**(10), 1690 (1999)
52.90 H.R. Kerp, E.E. van Faassen: Chem. Phys. Lett. **332**(1/2), 5 (2000)
52.91 P.D. Hooper, M.I. Newton, G. McHaleand, M.R. Willis: Semicond. Sci. Technol. **12**, 455 (1997)
52.92 D. Markovitsi, T.H. Tran-Thi, R. Even, J. Simon: Chem. Phys. Lett. **137**, 107 (1987)
52.93 T. Basova, E. Kol'tsov, A.K. Hassan, A. Nabok, A.G. Gurek, A.K. Ray, V. Ahsen: J. Mater. Sci. Mater. Electron. **15**(9), 623 (2004)
52.94 W. Snow, W.R. Barger: Phthalocyanine films in chemical sensors. In: *Phthalocyanines. Properties and Applications*, ed. by C.C. Leznoff, A.B.P. Lever (Wiley, New York 1989)
52.95 M. Nicolau, B. del Rey, T. Torres, C. Mingotaud, P. Delhaes, M.J. Cook, S.C. Thorpe: Synth. Met. **102**(1–3), 1462 (1999)
52.96 R. Zhou, F. Josse, W. Gopel, Z.Z. Öztürk, Ö. Bekaroğlu: Appl. Organomet. Chem. **10**, 557 (1996)
52.97 A. Chyla, A. Lewandowska, J. Soloducho, A. Gorecka-Drzazga, M. Szablewski: IEEE Trans. Dielect. El In **8**(3), 559 (2001)
52.98 S. Gao, H. Zhao, L.H. Huo, J.G. Zhao, Y.Q. Wu, S.Q. Xi: Sensors Actuat. B Chem. **97**(2/3), 319 (2004)
52.99 S. Suslick, N.A. Rakow, M.E. Kosal, J.-H. Chou: J. Porphyr. Phthalocyan. **4**, 407 (2001)
52.100 Y. Lee, B.K. Oh, M.E. Meyerhoff: Anal. Chem. **76**(3), 536 (2004)
52.101 J. Charvatova, O. Rusin, V. Kral, K. Volka, P. Matejka: Sensors Actuat. B **76**(1–3), 366 (2001)
52.102 O. Ikeda, H. Koyama, K. Kijima, T. Komura, A. Itajima, M. Miyake, K. Yamamoto, A. Yamatodani: Detection of Nitric Oxide with the Iron-Porphyrin Doped (III) Nafion|Glassy Carbon Electrode. In: *Proc. 27th Chem. Sensor Symp*, Vol. 14 (Supplement B), (Japan Association of Chemical Sensor, Nagaoka University of Technology 1998) p. 89
52.103 V.C. Smith, T. Richardson, H.L. Anderson: Supramolec. Sci. **4**(3/4), 503 (1997)
52.104 V. Arima, R.I.R. Blyth, F. Della Sala, R. Del Sole, F. Matino, G. Mele, G. Vasapollo, R. Cingolani: Mater. Sci. Eng. C Bio. Solids **24**(4), 569 (2004)
52.105 H. Imahori, K. Hosomizu, Y. Mori, T. Sato, T.K. Ahn, S.K. Kim, D. Kim, Y. Nishimura, I. Yamazaki, H. Ishii, H. Hotta, Y. Matano: J. Phys. Chem. B **108**(16), 5018 (2004)
52.106 Q.L. Li, S. Surthi, G. Mathur, S. Gowda, Q. Zhao, T.A. Sorenson, R.C. Tenent, K. Muthukumaran, J.S. Lindsey, V. Misra: Appl. Phys. Lett. **85**(10), 1829 (2004)
52.107 K.E. Splan, J.T. Hupp: Langmuir **20**(24), 10560 (2004)
52.108 J.R.C. da Rocha, G.J.F. Demets, M. Bertotti, K. Araki, H.E. Toma: J. Electroanal. Chem. **526**(1/2), 69 (2002)
52.109 J.D. Wright: Prog. Surf. Sci. **31**(1/2), 1 (1989)
52.110 J.P. Germain, A. Pauly, C. Maleysson, J.P. Blanc, B. Schöllhorn: Thin Solid Films **333**, 235 (1998)

52.111 B. Schöllhorn, J.P. Germain, A. Pauly, C. Maleysson, J.P. Blanc: Thin Solid Films **326**, 245 (1998)
52.112 J. Travis, A.K. Ray, S.C. Thorpe, M.J. Cook, S.A. James: Meas. Sci. Technol. **6**(7), 988 (1995)
52.113 A. Cole, R.J. McIlroy, S.C. Thorpe, M.J. Cook, J. McMurdo, A.K. Ray: Sensors Actuat. B **13**, 416 (1993)
52.114 D. Crouch, S.C. Thorpe, M.J. Cook, I. Chambrier, A.K. Ray: Sensors Actuat. B **18–19**, 411 (1994)
52.115 A. Tepore, A. Serra, D.P. Arnold, D. Manno, G. Micocci, A. Genga, L. Valli: Langmuir **17**(26), 8139 (2001)
52.116 Y.L. Lee, C.Y. Sheu, R.H. Hsiao: Sensors Actuat. B Chem **99**(2/3), 281 (2004)
52.117 Y.L. Lee, C.H. Hsiao, C.H. Chang, Y.M. Yang: Sens. Actuat. B **94**, 169 (2003)
52.118 M.I. Newton, T.K.H. Starke, G. McHale, M.R. Willis: Thin Solid Films **360**(1/2), 10 (2000)
52.119 M.I. Newton, T.K.H. Starke, M.R. Willis, G. McHale: Sens. Actuat. B **67**, 307 (2000)
52.120 Q. Zhou, R.D. Gould: Thin Solid Films **317**(1/2), 436 (1998)
52.121 W.F. Qiu, W.P. Hu, Y.Q. Liu, S.Q. Zhou, Y. Xu, D.B. Zhu: Sensors Actuat, B Chem. **75**(1/2), 62 (2001)
52.122 M. Bouvet, A. Leroy, J. Simon, F. Tournilhac, G. Guillaud, P. Lessnick, A. Maillard, S. Spirkovitch, M. Debliquy, A. Haan, A. Decroly: Sensors Actuat, B Chem. **72**(1), 86 (2001)
52.123 M. Bouvet, G. Guillaud, A. Leroy, A. Maillard, S. Spirkovitch, F.G. Tournilhac: Sensors Actuat, B Chem. **73**(1), 63 (2001)
52.124 C.Q. Sun, Y.P. Sun, X. Zhang, H.D. Xu, J.C.K. Shen: Anal. Chim. Acta **312**(2), 207 (1995)
52.125 Y.P. Sun, X. Zhang, C.Q. Sun, Z.Q. Wang, J.C. Shen, D.J. Wang, T.J. Li: Chem. Commun. **20**, 2379 (1996)
52.126 K.F. Schoch, J. Greggi, T.A. Temofonte: J. Vac. Sci. Technol. A **6**(1), 155 (1988)
52.127 A.K. Hassan, A.K. Ray, J.R. Travis, Z. Ghassemlooy, M.J. Cook, A. Abass, R.A. Collins: Sensors Actuat. B Chem. **49**(3), 235 (1998)
52.128 J. Mårtensson, H. Arwin, I. Lundstrom: Sensors Actuat. B Chem. **1**(1–6)), 134 (1990)
52.129 J.M. Pedrosa, C.M. Dooling, T.H. Richardson, R.K. Hyde, C.A. Hunter, M.T. Martin, L. Camacho: J. Mater. Chem. **12**(9), 2659 (2002)
52.130 O. Worsfold, C.M. Dooling, T.H. Richardson, M.O. Vysotsky, R. Tregonning, C.A. Hunter, C. Malins: Colloid Surf. A **198**, 859 (2002)
52.131 L. Gaffo, O.D.D. Couto, R. Giro, M.J.S.P. Brasil, D.S. Galvao, F. Cerdeira, O.N. de Oliveira, K. Wohnrath: Solid State Commun. **131**(1), 53 (2004)
52.132 T. Richardson, V.C. Smith, A. Topacli, J. Jiang, C.H. Huang: Supramol. Sci. **4**, 465 (1997)
52.133 T.R.E. Simpson, M.J. Cook, M.C. Petty, S.C. Thorpe, D.A. Russell: Analyst **121**(10), 1501 (1996)
52.134 T.R.E. Simpson, D.J. Revell, M.J. Cook, D.A. Russell: Langmuir **13**(3), 460 (1997)
52.135 E. Kretschmann: Z. Phys. **241**, 313 (1971)
52.136 I. Pockrand: Surf. Sci. **72**, 577 (1978)
52.137 J.M. Rooney, E.A.H. Hall: Anal. Chem. **76**(23), 6861 (2004)
52.138 T. Basova, E. Kol'tsov, A. Hassan, A. Tsargorodskaya, A.K. Ray, I. Igumenov: Phys. Stat. Sol. (b) **242**(4), 822 (2005)
52.139 J.D. Wright, A. Cado, S.J. Peacock, V. Rivalle, A.M. Smith: Sens. Actuat. B **29**, 108 (1995)
52.140 J.P. Lloyd, C. Pearson, M.C. Petty: Thin Solid Films **160**(1/2), 431 (1988)
52.141 M.J. Jory, P.S. Cann, J.R. Sambles: J. Phys. D **27**(1), 169 (1994)
52.142 K. Kato, C.M. Dooling, K. Shinbo, T.H. Richardson, F. Kaneko, R. Tregonning, M.O. Vysotsky, C.A. Hunter: Colloid Surf. A **198**, 811 (2002)
52.143 D.S. Ballantine, R.M. White, S.I. Martin, A.J. Ricco, E.T. Zellers, G.C. Fry, H. Wohltjen: *Acoustic Wave Sensors. Theory, Design, and Physico-Chemical Applications* (Academic Press, New York 1997)
52.144 K.D. Schierbaum, R. Zhou, S. Knecht, R. Dieing, M. Hanack, W. Göpel: Sensors Actuat. B **24**, 69 (1995)
52.145 H. Ding, V. Erokhin, M.K. Ram, S. Paddeu, L. Valkova, C. Nikolini: Thin Solid Films **379**, 279 (2000)
52.146 Z.Z. Öztürk, R. Zhou, U. Weimar, V. Ahsen, O. Bekaroğlu, W. Göpel: Sensors Actuat. B Chem. **26–27**, 208 (1995)
52.147 J. Souto, M.L. Rodriguez, J.A. Desaja, R. Aroca: Int. J. Electron. **76**(5), 763 (1994)
52.148 T. Basova, C. Tasaltin, A.G. Gurek, M.A. Ebeoğlu, Z.Z. Öztürk, V. Ahsen: Sensors Actuat. B Chem. **96**(1/2), 70 (2003)
52.149 C. Bariain, I.R. Matias, C. Fernandez-Valdivielso, F.J. Arregui, M.L. Rodriguez-Mendez, J.A. de Saja: Sensors Actuat. B Chem **93**(1–3), 153 (2003)
52.150 J. Spadavecchia, G. Ciccarella, R. Rella, S. Capone, P. Siciliano: Sensors Actuat. B Chem. **96**(3), 489 (2003)
52.151 J. Spadavecchia, G. Ciccarella, A. Buccolieri, G. Vasapollo, R. Rella: J. Porphyr. Phthalocyan. **7**(8), 572 (2003)
52.152 S. Nardis, D. Monti, C. Di Natale, A. D'Amico, P. Siciliano, A. Forleo, M. Epifani, A. Taurino, R. Rella, R. Paolesse: Sensors Actuat. B Chem. **103**(1/2), 339 (2004)
52.153 J. Spadavecchia, G. Ciccarella, G. Vasapollo, P. Siciliano, R. Rella: Sensors Actuat. B Chem. **100**(1/2), 135 (2004)
52.154 C. Granito, J.N. Wilde, S. Houghton, P.J. Iredale: Thin Solid Films **284/285**, 98 (1996)
52.155 E.K. Quirk, R. Mogg, D.D. Brown, M.A. Lally, D.V. Mehrotra, M.J. DiNubile, M.N. Robertson: Clin. Infect. Dis. **47**(12), 1593 (2008)
52.156 J.D. Huang, S.Q. Wang, P.C. Lo, W.P. Fong, W.H. Ko, D.K.P. Ng: New. J. Chem. **28**, 348 (2004)
52.157 T. Basova, S. Paul, D. Paul, P. Vadgama, A.G. Gürek, V. Ahsen, A.K. Ray: J. Bionanosci. **2**, 114 (2008)
52.158 S. Paul, D. Paul, T. Basova, A.K. Ray: J. Phys. Chem. C **112**(31), 11822 (2008)
52.159 S. Paul, D. Paul, T. Basova, A.K. Ray: IET Nanobiotechnology **4**(1), 1 (2010)
52.160 T. Basova, A.G. Gurek, V. Ahsen, A. Ray: Opt. Mater. **35**(3), 634 (2013)
52.161 G. Jin, C.O. Too, J. Norrish, G.G. Wallace: Synth. Met. **135**(1–3)), 29 (2003)

52.162 V. Papes, S. Brodska: Sensors Actuat. B Chem. **40**, 143 (1997)
52.163 A. Riul, A.M.G. Soto, S.V. Mello, S. Bone, D.M. Taylor, L.H.C. Mattoso: Synth. Met. **132**(2), 109 (2003)
52.164 J.S. Do, W.B. Chang: Sensors Actuat. B Chem. **101**(1/2), 97 (2004)
52.165 G. Anitha, E. Subramanian: Sensors Actuat. B Chem. **92**(1/2), 49 (2003)
52.166 E. Segal, R. Tchoudakov, M. Narkis, A. Siegmann, Y. Wei: Sensors Actuat. B Chem. **104**(1), 140 (2005)
52.167 E. Milella, F. Musio, M.B. Alba: Thin Solid Films **285**, 908 (1996)
52.168 Y. Kunugi, K. Nigorikawa, Y. Harima, K. Yamashita: J. Chem. Soc. Chem. Commun. **1994**(7), 873 (1994)
52.169 S. Christie, E. Scorsone, K. Persaud, F. Kvasnik: Sensors Actuat. B Chem. **90**(1–3)), 163 (2003)
52.170 M. Ando, C. Swart, E. Pringsheim, V.M. Mirsky, O.S. Wolfbeis: Solid State Ionics **152–153**, 819 (2002)
52.171 A. Penza, G. Cassano, A. Sergi, C. Lo Sterzo, M. Russo: Sensors Actuat. B Chem. **81**(1), 88 (2001)
52.172 T.A. Dickinson, J. White, J.S. Kauer, D.R. Walt: Nature **382**, 697 (1996)
52.173 D. Li, C.A. Mills, J.M. Cooper: Sensors Actuat. B Chem. **92**(1/2), 73 (2003)
52.174 T. Jeong, H.K. Lee, D.C. Jeong, S. Jeon: Talanta **65**(2), 543 (2005)
52.175 M.M. Ardakany, A.A. Ensafi, H. Naeimi, A. Dastanpour, A. Shamlli: Sensors Actuat. B Chem. **96**(1/2), 441 (2003)
52.176 S.Y. Huan, C.X. Jiao, Q. Shen, J.H. Jiang, G.M. Zeng, H.H. Guo, S.L. Guo, R.Q. Yu: Electrochim. Acta **49**(25), 4273 (2004)
52.177 P.A. Antunes, C.M. Santana, R.F. Aroca, O.N. Oliveira, C.J.L. Constantinoa, A. Riul: Synth. Met. **148**(1), 21 (2005)
52.178 T. Shimanouchi, S. Morita, H.S. Jung, Y. Sakurai, Y. Suzuki, R. Kuboi: Sensor Mater **16**(5), 255 (2004)
52.179 P.C. Ewbank, R.S. Loewe, L. Zhai, J. Reddinger, G. Sauve, R.D. McCullough: Tetrahedron **60**(49), 11269 (2004)
52.180 J.N. Wilde, J. Nagel, M.C. Petty: Thin Solid Films **327–329**, 726 (1998)
52.181 R. Casalini, J.N. Wilde, J. Nagel, U. Oertel, M.C. Petty: Sensors Actuat. B **57**, 28 (1999)
52.182 J.K. Abraham, B. Philip, A. Witchurch, V.K. Varadan, C.C. Reddy: Smart Mater. Struct. **13**(5), 1045 (2004)
52.183 B. Philip, J.K. Abraham, A. Chandrasekhar, V.K. Varadan: Smart Mater. Struct. **12**(6), 935 (2003)
52.184 R. Capan, A.K. Ray, A.K. Hassan, T. Tanrisever: J. Phys. D Appl. Phys. **36**, 1115 (2003)
52.185 R. Rego, N. Caetanoc, R. Vale, A. Mendes: J. Membr. Sci. **244**(1–2), 35–44 (2004)
52.186 M. Matsuguchi, A. Okamoto, Y. Sakai: Sensors Actuat. B Chem. **94**(1), 46 (2003)
52.187 J. Sutter, A. Radu, S. Peper, E. Bakker, E. Pretsch: Anal. Chim. Acta **523**(1), 53 (2004)
52.188 C. Ramesh, G. Velayutham, N. Murugesan, V. Ganesan, V. Manivannan, G. Periaswami: Ionics **10**(1/2), 50 (2004)
52.189 A. Calogirou, M. Duan, D. Kotzias, M. Lahaniati, B.R. Larsen: Atmos. Environ. **31**, 2741 (1997)
52.190 A.V. Nabok, A.K. Hassan, A.K. Ray, J. Travis, M. Hofton, A. Dalley: IEE Proc. Sci. Meas. Technol. **147**, 153 (2000)
52.191 A.K. Ray, A.V. Nabok, A.K. Hassan, M. Hofton, A. Dalley: Polyphenylsulphide thin films prepared by spin coating for ozone detection. In: *Sensors and their Appl. X Conf*, ed. by N.M. White, J.T. Augousti (1999)
52.192 A.K. Hassan, A.V. Nabok, A.K. Ray, G. Kiousis: Mater. Sci. Eng. C **22**, 197 (2002)
52.193 A.K. Hassan, J. Greenway, A.K. Ray, A.V. Nabok: J. Phys. D Appl. Phys. **36**(17), 2130 (2003)
52.194 B. Ding, J.H. Kim, Y. Miyazaki, S.M. Shiratori: Sensors Actuat. B Chem. **101**(3), 373 (2004)
52.195 L. Uzun, A.P.F. Turner: Biosens. Bioelectron. **76**(SI), 131 (2016)
52.196 J.D. Marty, M. Mauzac: Adv. Polym. Sci. **172**, 1 (2005)
52.197 H. Sambe, K. Hoshina, J. Haginaka: J. Chromatogr. A **1152**(1/2), 130 (2007)
52.198 R.A. Abram, S. Brand: J. Phys. D **48**(12), 125101 (2015)
52.199 Z. Cao, D. Cao, Z.G. Lei, H.G. Lin, R.Q. Yu: Talanta **44**, 1413 (1997)
52.200 C.D. Gutsche: *Calixarenes* (Royal Society of Chemistry, Cambridge 1989)
52.201 D.J. Cram, S. Karbach, H.–E. Kim, C.B. Knober, E.F. Maverick, J.L. Ericson, R.C. Hegelson: J. Am. Chem. Soc. **110**, 2229 (1988)
52.202 F.L. Dickert, U.P.A. Baumler, G.K. Zwissler: Synth. Met. **61**, 47 (1993)
52.203 P. Nelli, E. Delcanale, G. Faglia, G. Sberveglieri, P. Soncini: Sensors Actuat. B Chem. **13/14**, 302 (1993)
52.204 T. Weiss, K.D. Schierbaum, W. Göpel, U. Thoden van Velzen, U. Thoden van Velzen: U. Thoden van Velzen, D. N. Reinhoudt, Sensors Actuat. B Chem **26**, 203 (1995)
52.205 E. Dalcanale, J. Hartman: Sensors Actuat. B Chem. **24**, 39 (1995)
52.206 J. Rickert, T. Weiss, W. Gopel: Sensors Actuat. B Chem **31**, 45 (1996)
52.207 A.K. Hassan, A.K. Ray, A.V. Nabok, F. Davis: Sensors Actuat. B **77**, 638 (2001)
52.208 A.V. Nabok, N.V. Lavrik, Z.I. Kazantseva, B.A. Nesterenko, L.N. Markovskiy, V.I. Kalchenko, A.V. Shivaniuk: Thin Solid Films **259**, 244 (1995)
52.209 A.V. Nabok, A.K. Hassan, A.K. Ray: J. Mater. Chem. **10**, 189 (2000)
52.210 A.V. Nabok, A.K. Hassan, A.K. Ray, O. Omar, V.I. Kalchenko: Sensors Actuat. B Chem. **45**, 115 (1997)
52.211 A.K. Hassan, A.K. Ray, A.V. Nabok, T. Wilkop: Appl. Surf. Sci. **182**, 49 (2001)
52.212 S.J. Gregg, K.S.W. Sing: *Adsorption, Surface Area and Porosity* (Academic Press, New York 1967)
52.213 T. Wilkop, A.K. Ray: J. Phys. D Appl. Phys. **35**(20), 2661 (2002)
52.214 P. Gouma, G. Sberveglieri, R. Dutta, J.W. Gardner, E.L. Hines: MRS Bull. **29**(10), 697 (2004)

52.215 A.V. Shevade, M.A. Ryan, M.L. Homer, A.M. Manfreda, H. Zhou, K.S. Manatt: Sensors Actuat. B Chem **93**(1–3), 84 (2003)
52.216 A. Mills, S.L. Hunte: J. Photochem. Photobiol. A **108**, 1 (1997)
52.217 G.J. Wilson, G.D. Will: Curr. Appl. Phys. **4**(2–4), 351 (2004)
52.218 D. Chatterjee, A. Mahata: J. Photochem. Photobiol. **153**(1–3), 199 (2002)
52.219 L.R. Skubal, N.K. Meshkov, M.C. Vogt: J. Phototechnol. Photobiol. A **148**(1–3), 103 (2002)